

# Sampling the volatile-rich transition zone beneath Bermuda

Sarah E. Mazza<sup>1</sup>\*, Esteban Gazel<sup>2</sup>\*, Michael Bizimis<sup>3</sup>, Robert Moucha<sup>4</sup>, Paul Béguelin<sup>3</sup>, Elizabeth A. Johnson<sup>5</sup>, Ryan J. McAleer<sup>6</sup> & Alexander V. Sobolev<sup>7,8</sup>

Intraplate magmatic provinces found away from plate boundaries provide direct sampling of the composition and heterogeneity of the Earth's mantle. The chemical heterogeneities that have been observed in the mantle are usually attributed to recycling during subduction<sup>1-3</sup>, which allows for the addition of volatiles and incompatible elements into the mantle. Although many intraplate volcanoes sample deep-mantle reservoirs-possibly at the coremantle boundary<sup>4</sup>—not all intraplate volcanoes are deep-rooted<sup>5</sup>, and reservoirs in other, shallower boundary layers are likely to participate in magma generation. Here we present evidence that suggests Bermuda sampled a previously unknown mantle domain, characterized by silica-undersaturated melts that are substantially enriched in incompatible elements and volatiles, and a unique, extreme isotopic signature. To our knowledge, Bermuda records the most radiogenic <sup>206</sup>Pb/<sup>204</sup>Pb isotopes that have been documented in an ocean basin (with <sup>206</sup>Pb/<sup>204</sup>Pb ratios of 19.9-21.7) using highprecision methods. Together with low <sup>207</sup>Pb/<sup>204</sup>Pb ratios (15.5–15.6) and relatively invariant Sr, Nd, and Hf isotopes, the data suggest that this source must be less than 650 million years old. We therefore interpret the Bermuda source as a previously unknown, transient mantle reservoir that resulted from the recycling and storage of incompatible elements and volatiles<sup>6-8</sup> in the transition zone (between the upper and lower mantle), aided by the fractionation of lead in a mineral that is stable only in this boundary layer, such as K-hollandite<sup>9,10</sup>. We suggest that recent recycling into the transition zone, related to subduction events during the formation of Pangea, is the reason why this reservoir has only been found in the Atlantic Ocean. Our geodynamic models suggest that this boundary layer was sampled by disturbances related to mantle flow. Seismic studies and diamond inclusions<sup>6,7</sup> have shown that recycled materials can be stored in the transition zone<sup>11</sup>. For the first time, to our knowledge, we show geochemical evidence that this storage is key to the generation of extreme isotopic domains that were previously thought to be related only to deep recycling.

The island of Bermuda is the surficial expression of a 1,500-km-long topographic swell, which trends northeast to southwest and rises 1 km above 110–140-Myr-old oceanic crust<sup>12</sup> (Fig. 1a). Like many ocean volcanic islands, Bermuda has been historically explained as being derived from a mantle plume<sup>13</sup>; however, evidence that supports the plume model is not conclusive. A first-order problem is the lack of a hotspot track associated with Bermuda<sup>12</sup>. Bermuda is the only visible volcanic feature in the proximity of the proposed hotspot trail, and there is no evidence for volcanism at the proposed current location of the hotspot, approximately 650 km southeast of Bermuda (Extended Data Fig. 1). The transition zone beneath Bermuda is 27 km thinner than the global average, due to the combined effects of a depressed 410 km discontinuity and a depressed 660 km discontinuity, and this has been used as evidence to argue both in favour of and against

the mantle plume model for Bermuda<sup>14</sup>. More recent geodynamic models propose that edge-driven convection—a small-scale convection associated with the thermal contrast between thick (cold) continental lithosphere and thin (warm) oceanic lithosphere—provides an alternative, plume-absent mechanism for the formation of Bermuda<sup>14,15</sup>.

Present-day mantle structure in the North Mid-Atlantic, as inferred from global joint seismic-geodynamic models<sup>16</sup>, reveals an organized thermal anomaly in the upper mantle beneath Bermuda that extends down to mid-mantle depths. Numerical models of present-day global mantle flow, driven by density inferred from these joint seismicgeodynamic inversions, indicate that this thermal anomaly is actively rising through the transition zone (Fig. 1b, d). To simulate the position of this thermal anomaly 30 Myr ago, we advected the global mantle flow model backwards by 30 Myr in order to coincide with active volcanism at Bermuda. We note that in this approach we neglect thermal diffusion, and thus the retrodicted warm mantle anomaly will be cooler than in our simulations. There are also limitations associated with the reconstruction of thermal anomalies that initially had a relatively small footprint in the mantle (less than 100 km) or that have since diffused into the upper-mantle thermal boundary. Nonetheless, at 30 Myr ago, we observe mantle flow with an upward component beneath the Bermuda region that samples both the transition zone and mid-mantle depths (Fig. 1c, e). Even though the reconstructed mantle anomalies are cooler than those observed today, it is reasonable to assume that these thermal anomalies were hotter, because they resulted in active volcanism 30 Myr ago.

To test whether Bermuda sampled source reservoirs in the transition zone, we produced the first, to our knowledge, comprehensive geochemical study of the 767 m record of continuous igneous activity recovered by the Deep Drill 1972 borehole<sup>17</sup>. We found that Bermuda is composed of two interbedded lithologies: a silica-undersaturated alkaline suite (SiO<sub>2</sub> < 42.4 wt%), and a silica-saturated suite (SiO<sub>2</sub>: 49.7–52.9wt %) (Fig. 2a, Extended Data Fig. 2; see Methods for a full discussion of core stratigraphy and mineralogy). Argonargon (40Ar/39Ar) dating of phlogopite separates from three of the silica-undersaturated units reveals ages of approximately 30.9 Myr (Extended Data Fig. 3, Supplementary Table 1). When normalized to primitive mantle, these samples show characteristic patterns expected of ocean island basalts—especially the HIMU (high <sup>238</sup>U/<sup>204</sup>Pb ratio) type with enrichments in incompatible elements—and substantial negative anomalies in fluid-mobile elements such as K and Pb (Fig. 2b, Supplementary Table 2). Our data clearly show that Bermuda silica-undersaturated units are the most trace-element-enriched silicate magmas in the Atlantic, and are more enriched than classic HIMU magmas (Extended Data Fig. 4). The silica-saturated units are relatively depleted in trace elements (Fig. 2b), but they are still more geochemically enriched than the surrounding local basaltic oceanic

<sup>1</sup>Institute for Planetology, University of Münster, Münster, Germany. <sup>2</sup>Department of Earth and Atmospheric Sciences, Cornell University, Ithaca, NY, USA. <sup>3</sup>School of Earth, Ocean and the Environment, University of South Carolina, Columbia, SC, USA. <sup>4</sup>Department of Earth Sciences, Syracuse University, Syracuse, NY, USA. <sup>5</sup>Department of Geology and Environmental Science, James Madison University, Harrisonburg, VA, USA. <sup>6</sup>Florence Bascom Geoscience Center, United States Geological Survey, Reston, VA, USA. <sup>7</sup>Univ. Grenoble Alpes, Univ. Savoie Mont Blanc, CNRS, IRD, IFSTTAR, ISTerre, Grenoble, France. <sup>8</sup>Vernadsky Institute of Geochemistry and Analytical Chemistry, Russian Academy of Sciences, Moscow, Russia. \*e-mail: smazza@smith.edu; egazel@cornell.edu

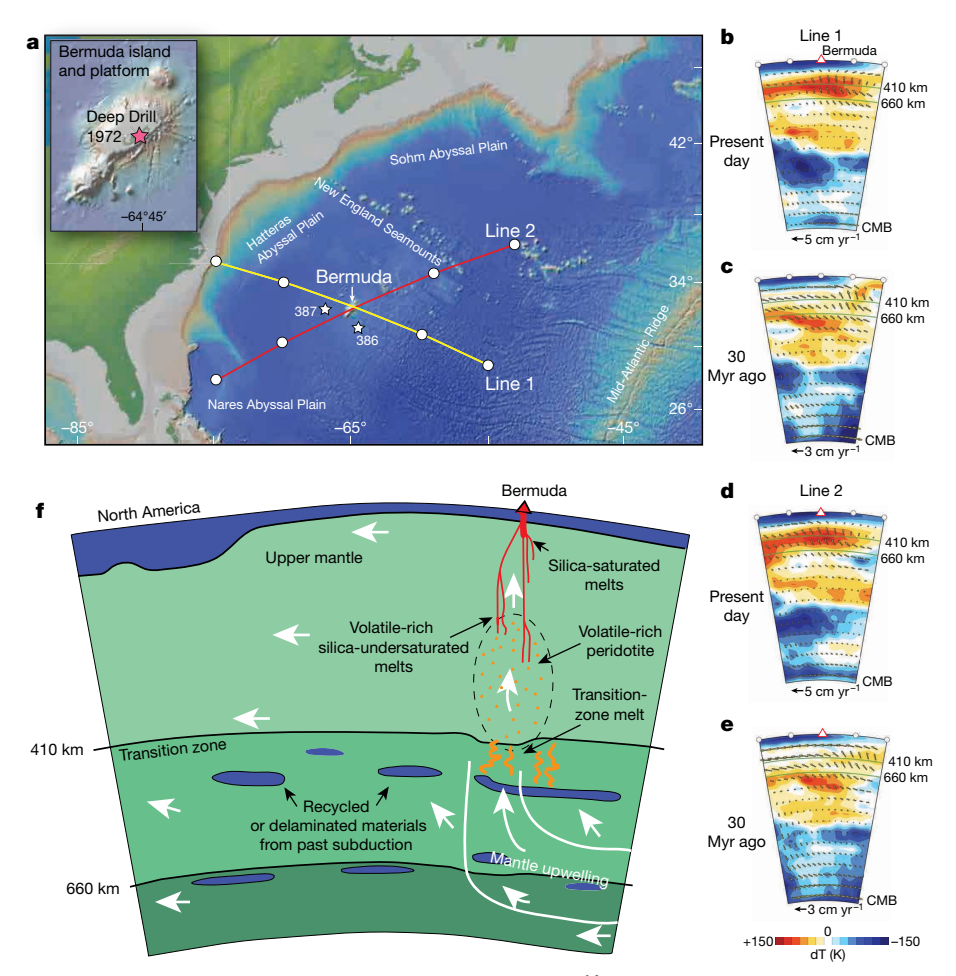


**Fig. 1** | **Map, geodynamic and schematic models of Bermuda. a,** Map of the Atlantic Ocean indicating the location of Bermuda, the Deep Drill 1972 borehole, and the two cross-sectional lines used for geodynamic modelling, modified from http://www.geomapapp.org<sup>35</sup>. **b, d,** Present-day mantle flow and thermal heterogeneity cross-section, inferred from joint seismic–geodynamic model TX2008 with mantle viscosity V2 following ref. <sup>16</sup>, for lines 1 and 2 shown in **a. c, e,** Corresponding reconstructed mantle flow and thermal heterogeneity at 30 Myr ago using backward

advection<sup>16</sup> (note the different flow-velocity scale compared to the present day). **f**, Schematic model to explain the volcanism of Bermuda as a product of small convection in the upper mantle. White lines and arrows represent mantle flow as modelled by **b**-**e**, which samples both the volatile-rich peridotite and the depleted upper mantle. Depressions at 410 km and 660 km are not drawn to scale, but approximate previous observation<sup>14</sup>. Recycled material at the base of the transition zone represents trapped subducted crust from previous models<sup>34</sup>. CMB, core–mantle boundary.

crust<sup>18</sup> (see Methods for a discussion of the relationship between silica-undersaturated and silica-saturated units).

Olivines from the silica-undersaturated magmas have forsterite (molar Mg/(Mg + Fe)  $\times$  100%) contents ranging from 84.3% to 88.8%; in addition, the concentration of Ni and the Fe/Mn ratio are low whereas Ca concentrations are high, suggesting that the olivine most likely crystallized from a peridotite-sourced melt<sup>19</sup> (Fig. 3). Olivines from the archetype HIMU magmas of Mangaia are also characterized by high Ca and low Al concentrations, which are interpreted as resulting from interaction and enrichment with primary carbonatitic melts<sup>20</sup>. Our new high-precision analyses from Bermuda olivines reveal an average Ca content greater than the most Ca-rich olivine from Mangaia (3,455 p.p.m. compared with 3,224 p.p.m., respectively). Before this study, Mangaia had recorded the highest known Ca content in olivine from an oceanic island, which was interpreted as the result of magmas sampling a source that has been metasomatized by carbon-rich fluids<sup>20</sup> (Fig. 3). We estimated minimum olivine crystallization temperatures via olivine-spinel thermometry, which is based on the exchange of  $Al_2O_3$  between forsterite-rich olivine (forsterite content  $\geq 88\%$ ) and Cr-rich spinels<sup>21</sup> of 1,253  $\pm$  10 °C for Bermuda (Supplementary Table 2). These results are more consistent with temperatures for upper ambient mantle-derived melts (1,270 °C) than with plume-derived magmas with crystallization temperatures (1,353–1,485 °C)<sup>21</sup> from materials sourced at the core-mantle boundary.

Silica-undersaturated, alkaline magmas with SiO<sub>2</sub> contents less than 43 wt% cannot be produced by simple peridotite mantle melting, and several hybrid sources for these magmas have been proposed on the basis of various experiments: carbonated peridotite<sup>22,23</sup>, eclogite and garnet pyroxenite<sup>24</sup>, and carbonated eclogite<sup>25</sup>. Given the similarities in major elements from the experimental datasets—especially high CaO coupled with low SiO<sub>2</sub><sup>23</sup> (Fig. 2c, Extended Data Fig. 5; see Methods for details)—our new Bermuda data can be explained by the melting of a carbonated peridotite. The residual garnet lowers the concentration of Al<sub>2</sub>O<sub>3</sub> and heavy rare-earth elements in the melt<sup>25</sup>; both of these geochemical signatures are preserved in Bermuda silica-undersaturated lavas (for example, low Al<sub>2</sub>O<sub>3</sub> in olivines and lavas, and a steep slope in heavy rare-earth elements, Fig. 2b). Additionally, the presence of phases such as apatite, phlogopite, Ti-augite and perovskite are also consistent with the melting of a metasomatized, volatile-rich source<sup>26</sup>. Finally, magmatic water concentrations in equilibrium with measured Bermuda clinopyroxene phenocrysts  $^{27,28}$  range from 1.9 wt% to 5.7 wt%, which is higher than that expected in intraplate volcanics (typical range 0.03-1.0 wt% water)<sup>27,29</sup>. The measured magmatic water content from clinopyroxene is in agreement with water contents estimated by using the H<sub>2</sub>O/Ce ratio of Atlantic intraplate magmas<sup>30</sup> (250) and the Ce concentrations collected in the Bermuda silica-undersaturated lavas, yielding an average of 5.2 wt% H<sub>2</sub>O. This supports a more volatile-rich

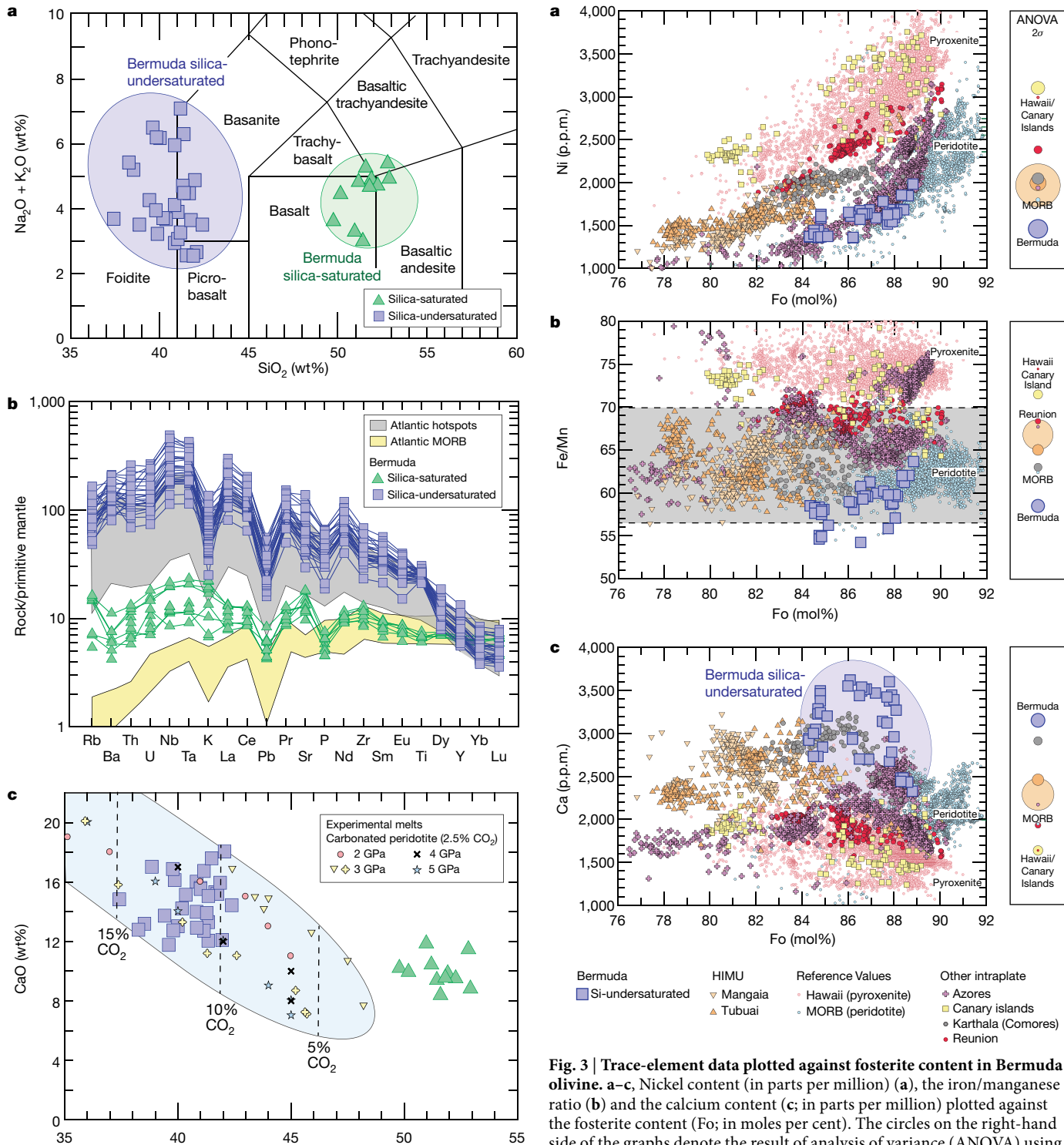


Fig. 2 | Bulk rock geochemistry of Bermuda. a, Total alkali content  $(Na_2O+K_2O)$  plotted against  $SiO_2$  content (in weight per cent). Regions containing silica-undersaturated and silica-saturated rocks are shaded in blue and green, respectively. b, Normalized trace element abundances in the primitive mantle for Bermuda, Atlantic mid-ocean-ridge basalt (MORB) (23°-33° N) and Atlantic hotspots from the Geochemistry of Rocks of the Oceans and Continents (GEOROC) database. c, Comparison of the CaO and SiO<sub>2</sub> contents (in weight per cent) of Bermuda with experimental data from melting carbonated peridotite and eclogite<sup>22,23</sup>. The blue shaded region contains experimental melts from a carbonated source, and the dashed lines indicate the stated percentage of CO2 in the primary melts.

SiO<sub>2</sub> (wt%)

olivine. a-c, Nickel content (in parts per million) (a), the iron/manganese ratio (b) and the calcium content (c; in parts per million) plotted against the fosterite content (Fo; in moles per cent). The circles on the right-hand side of the graphs denote the result of analysis of variance (ANOVA) using a Student's *t*-test at the 95% confidence interval for each location. The radii of the circles are proportional to the s.e.m. The grey shaded region in  ${\bf b}$ represents the Fe/Mn composition of peridotite. The blue shaded region in c contains the silica-unsaturated rocks from Bermuda. Olivine traceelement data are from the GEOROC database, ref. 19 and this study.

ANOVA

Canary

0

MORE

Reunion

MORB

Bermuda

Bermuda

MORB

Hawaii/

92

92

92

source for Bermuda than has been recorded in any other oceanic intraplate volcanoes<sup>29</sup> (see Methods for details).

As is the case with the major elements and trace elements, the data for radiogenic Pb, Sr, Nd and Hf isotopes require at least two different mantle sources for Bermuda. The silica-saturated magmas trend towards depleted mantle (Fig. 4). The silica-undersaturated units show clear similarities with HIMU-type mantle, as seen in the highly radiogenic <sup>206</sup>Pb/<sup>204</sup>Pb and <sup>208</sup>Pb/<sup>204</sup>Pb, and the less radiogenic <sup>143</sup>Nd/<sup>144</sup>Nd.

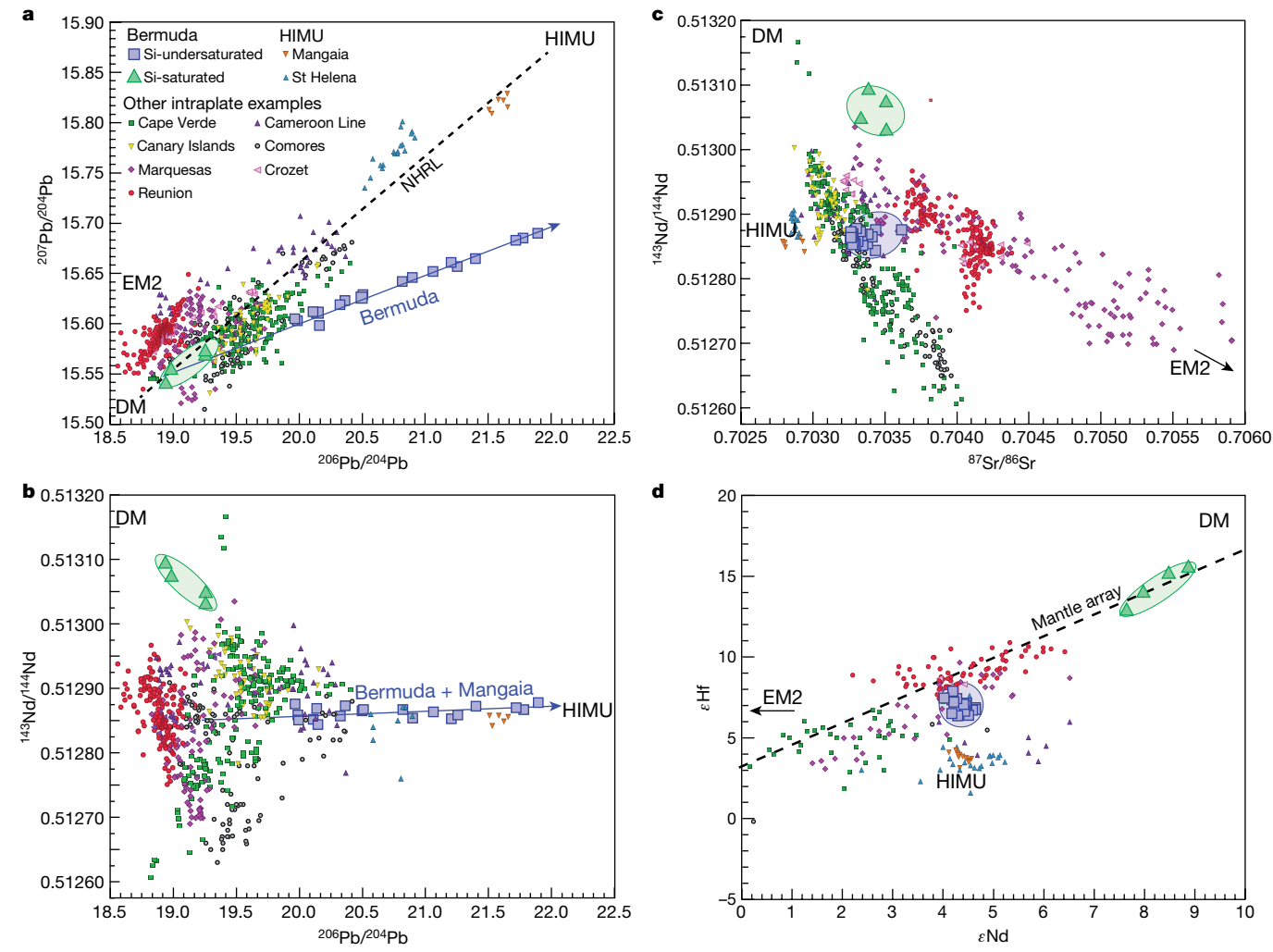


Fig. 4 | Pb, Sr, Nd and Hf isotopic composition of Bermuda lavas. Radiogenic isotopes for Bermuda compared with Mangaia, St Helena, Cape Verde, Cameroon Line, Canary Islands, Marquesas, Crozet, Comores and Reunion ocean island basalts. The data were obtained from the GEOROC database; Mangaia samples were limited to analyses obtained via multicollector inductively coupled plasma coupled to mass spectrometry. a,  $^{207}\text{Pb}/^{204}\text{Pb}$  plotted against  $^{206}\text{Pb}/^{204}\text{Pb}$ , showing a shallow slope for Bermuda silica-undersaturated samples, with  $^{206}\text{Pb}/^{204}\text{Pb}$  similar to that of Mangaia and St Helena. b,  $^{143}\text{Nd}/^{144}\text{Nd}$  plotted against  $^{206}\text{Pb}/^{204}\text{Pb}$ ,

showing invariable  $^{143}$ Nd/ $^{144}$ Nd in the silica-undersaturated samples with  $^{206}$ Pb/ $^{204}$ Pb more radiogenic than Mangaia. c,  $^{143}$ Nd/ $^{144}$ Nd plotted against  $^{87}$ Sr/ $^{88}$ Sr, showing near-consistent  $^{87}$ Sr/ $^{88}$ Sr for Bermuda with Bermuda silica-saturated having more radiogenic Nd. d,  $\varepsilon$ Hf against  $\varepsilon$ Nd showing Bermuda silica-undersaturated samples, plotting close below the mantle array. Regions containing silica-undersaturated and silica-saturated rocks are shaded in blue and green, respectively. DM, depleted mantle; EM2, enriched mantle 2; NHRL, Northern Hemisphere reference line.

The <sup>87</sup>Sr/<sup>86</sup>Sr of the silica-undersaturated lavas is slightly more radiogenic than that of the HIMU end-member, falling within the range of other Atlantic hotspots, whereas the <sup>176</sup>Hf/<sup>177</sup>Hf is closer to that of the mantle array than the HIMU end member (Fig. 4). The new data shows that <sup>206</sup>Pb/<sup>204</sup>Pb from Bermuda is more radiogenic than those from St Helena and Mangaia—the Atlantic and Pacific HIMU end members, respectively (Fig. 4a). However, in terms of the <sup>207</sup>Pb/<sup>204</sup>Pb, Bermuda is unique compared to all other ocean island basalts, as the values are considerably lower than typical HIMU values for a given <sup>206</sup>Pb/<sup>204</sup>Pb. Upon first observation, the shallow slope of all the samples age-corrected to 30 Myr ago in <sup>206</sup>Pb/<sup>204</sup>Pb-<sup>207</sup>Pb/<sup>204</sup>Pb space appears to be an isochron corresponding to an extremely young source (Extended Data Fig. 6, Methods). However, there is one key factor that makes this isochron unrealistic: an extremely high  $\mu$  value (where  $\mu$  is the <sup>238</sup>U/<sup>204</sup>Pb ratio) of up to 600 is required to explain the most radiogenic sample if the initial isotope value was similar to the least radiogenic sample; this is substantially higher than the highest measured value ( $\mu = 53$ ) in these lavas (Extended Data Fig. 7). The resulting extreme range of source  $\mu$  required to explain the variance of the undersaturated lavas (more than a factor of ten) is not seen in the lavas themselves,

where  $\mu$  varies by only a factor of two. Therefore, we suggest that the extreme Pb isotope signatures are likely to be the result of mixing between a moderately depleted source, similar to the one that melted to produce the Bermuda silica-saturated units, and a highly radiogenic end member ( $^{206}\text{Pb}/^{204}\text{Pb} > 21.5$ ).

The mixing end member of the silica-undersaturated units is likely to be more radiogenic than the most radiogenic sample analysed (B703); however, we can use this sample to calculate a minimum  $\mu$  for any possible mixing end member. Using a Monte Carlo simulation (see Methods for details) we constrained the possible combinations of source age and  $\mu$  values that can reproduce the Bermuda radiogenic  $^{206}\text{Pb}/^{204}\text{Pb}$ , with their characteristically low  $^{207}\text{Pb}/^{204}\text{Pb}$ . Our modelling suggests that the source age must be younger than 650 Myr with a minimum of  $\mu > 35$  and  $\Omega > 100$  ( $\Omega = ^{232}\text{Th}/^{204}\text{Pb}$ ). These models—combined with the lack of correlation in  $\varepsilon \text{Nd}$  and  $\varepsilon \text{Hf}$  (where  $\varepsilon \text{Nd}$  and  $\varepsilon \text{Hf}$  are the per ten thousand deviations from chondritic values of 0.512638 for  $^{143}\text{Nd}/^{144}\text{Nd}$  and 0.282772 for  $^{176}\text{Hf}/^{177}\text{Hf}$ ) and the invariable Lu/Hf (0.03–0.05) and Sm/Nd ratios (0.15–0.18)—suggest that the Bermuda silica-undersaturated magmas tap a young mantle domain, with extreme  $\mu$  and  $\Omega$  values, that has not been recorded before.

Lead isotopes in the classic HIMU mantle source are too radiogenic to originate from an undifferentiated mantle or from depleted upper-mantle peridotite<sup>31</sup>. Recycling of incompatible elements via subduction has been a crucial model for the production of the classic HIMU reservoir<sup>32</sup>. Recent hypotheses suggest that the HIMU signature results from mixing small-degree melts (carbonatitic and silicic) that are stored in the transition zone from subducted oceanic lithosphere<sup>31</sup>, or by melts from subduction-related carbon-rich metasomatized subcontinental lithospheric mantle<sup>20</sup>. In both scenarios the melt, which is enriched in incompatible elements, interacts with peridotite mantle to produce a metasomatized source that can derive silicaundersaturated, alkaline melts with phases such as Ti-augite, phlogopite, spinel, perovskite and apatite<sup>26</sup>—minerals that are clearly observed in our Bermuda samples (Extended Data Fig. 2). Globally, ocean island basalts trending towards the classic HIMU mantle are the most silica-undersaturated, and the highest <sup>206</sup>Pb/<sup>204</sup>Pb from Mangaia melt inclusions are associated with carbonate 'globules', which suggests a link between carbon in the mantle and the HIMU-like source compositions<sup>26</sup>. Bermuda is also characterized by highly fractionated incompatible elements (Extended Data Fig. 4), with higher than typical HIMU U/Pb, Th/Pb and Ce/Pb and lower than HIMU K/U and K/Nb. This suggests that trace-element-enriched signatures are not due to sulfide fractionation, and instead supports a recycling origin.

On the basis of the unique geochemical constraints, we suggest that the source of Bermuda is the product of recycling volatile-rich materials in the last 650 Myr, either during subduction that occurred with the amalgamation of Pangea or during delamination of metasomatized subcontinental lithospheric mantle that triggered the break-up of Pangea<sup>33</sup>. In either scenario, the recycled materials provided carbon and water-rich fluids that interacted with the ambient Atlantic upper mantle, possibly in the presence of a mineral phase such as K-hollandite. K-hollandite has been experimentally shown to markedly fractionate U/Pb and K/U ratios at transition zone depths during carbonate melt extraction<sup>9</sup>, and thus the residual K-hollandite retains the elements necessary to generate an enriched mantle signature<sup>10</sup>. The HIMU and the enriched mantle reservoir have been suggested to be physically related to subduction processes<sup>32</sup>, with the enriched mantle reservoir being the second stage of melting stagnant subducted slabs in the transition zone<sup>10</sup>. In this model, the carbonated melt that is rich in Th, U, and depleted in Pb is 'lost' in the transition zone<sup>10</sup>, and thus could be the missing link in the production of the HIMU signature that is observed in Bermuda. Furthermore, recent discoveries in diamond inclusions coupled with seismic and experimental data—provide evidence for a volatile-rich transition zone<sup>6-8</sup> associated with subducted slabs<sup>34</sup>. Our geodynamic models confirm a small-scale convective cell that sampled the transition zone below Bermuda, resulting in a unique geochemical composition that is characterized by an extreme HIMU-like signature. This suggests that the transition zone is more important than has been previously considered in the development of mantle heterogeneities, and that deep and ancient recycling is not the only mechanism for the generation of extreme isotopic mantle compositions.

#### Online content

Any methods, additional references, Nature Research reporting summaries, source data, statements of data availability and associated accession codes are available at https://doi.org/10.1038/s41586-019-1183-6.

Received: 1 October 2018; Accepted: 18 March 2019; Published online 15 May 2019.

- Chauvel, C., Lewin, E., Carpentier, M., Arndt, N. T. & Marini, J.-C. Role of recycled oceanic basalt and sediment in generating the Hf–Nd mantle array. *Nat. Geosci.* 1, 64–67 (2008).
- Hofmann, A. Mantle geochemistry: the message from oceanic volcanism. Nature 385, 219–229 (1997).
- Zindler, A. & Hart, S. Chemical geodynamics. Annu. Rev. Earth Planet. Sci. 14, 493–571 (1986).
- Rizo, H. et al. Preservation of Earth-forming events in the tungsten isotopic composition of modern flood basalts. Science 352, 809–812 (2016).
- Anderson, D. L. & King, S. D. Driving the Earth machine? Science 346, 1184–1185 (2014).

- Pearson, D. G. et al. Hydrous mantle transition zone indicated by ringwoodite included within diamond. *Nature* **507**, 221–224 (2014).
- Tschauner, O. et al. Ice-VII inclusions in diamonds: evidence for aqueous fluid in Earth's deep mantle. Science 359, 1136–1139 (2018).
- 8. Schmandt, B., Jacobsen, S. D., Becker, T. W., Liu, Z. & Dueker, K. G. Dehydration melting at the top of the lower mantle. *Science* **344**, 1265–1268 (2014).
- Grassi, D., Schmidt, M. W. & Günther, D. Element partitioning during carbonated pelite melting at 8, 13 and 22 GPa and the sediment signature in the EM mantle components. Earth Planet. Sci. Lett. 327–328, 84–96 (2012).
- Wang, X. J. et al. Mantle transition zone-derived EM1 component beneath NE China: Geochemical evidence from Cenozoic potassic basalts. *Earth Planet. Sci. Lett.* 465, 16–28 (2017).
- Ballmer, M. D., Schmerr, N. C., Nakagawa, T. & Ritsema, J. Compositional mantle layering revealed by slab stagnation at ~1000-km depth. Sci. Adv. 1, e1500815 (2015).
- Vogt, P. R. & Jung, W.-Y. in Plates, Plumes and Planetary Processes Vol. 430 (eds Foulger, G. R. & Jurdy, D. M.) 553–591 (Geological Society of America, 2007).
- Morgan, W. J. Hotspot tracks and the early rifting of the Atlantic. *Tectonophysics* 94, 123–139 (1983).
- Benoit, M. H., Long, M. D. & King, S. D. Anomalously thin transition zone and apparently isotropic upper mantle beneath Bermuda: Evidence for upwelling. Geochem. Geophys. Geosyst. 14, 4282–4291 (2013).
- King, S. D. & Anderson, D. L. Edge-driven convection. Earth Planet. Sci. Lett. 160, 289–296 (1998).
- Simmons, N. A., Forte, A. M. & Grand, S. P. Thermochemical structure and dynamics of the African super-plume. *Geophys. Res. Lett.* 34, L02301 (2007)
- Reynolds, P. & Aumento, F. Deep Drill 1972. Potassium–argon dating of the Bermuda drill core. Can. J. Earth Sci. 11, 1269–1273 (1974).
- Janney, P. E. & Castillo, P. R. Geochemistry of the oldest Atlantic oceanic crust suggests mantle plume involvement in the early history of the central Atlantic Ocean. Earth Planet. Sci. Lett. 192, 291–302 (2001).
- Sobolev, A. V. et al. The amount of recycled crust in sources of mantle-derived melts. Science 316, 412–417 (2007).
- Weiss, Y., Class, C., Goldstein, S. L. & Hanyu, T. Key new pieces of the HIMU puzzle from olivines and diamond inclusions. *Nature* 537, 666–670 (2016).
- Coogan, L., Saunders, A. & Wilson, R. Aluminum-in-olivine thermometry of primitive basalts: evidence of an anomalously hot mantle source for large igneous provinces. *Chem. Geol.* 368, 1–10 (2014).
- Dasgupta, R., Hirschmann, M. M. & Smith, N. D. Partial melting experiments of peridotite + CO<sub>2</sub> at 3 GPa and genesis of alkalic ocean island basalts. *J. Petrol.* 48, 2093–2124 (2007).
- Dasgupta, R. et al. Carbon-dioxide-rich silicate melt in the Earth's upper mantle. Nature 493, 211–215 (2013).
- Kogiso, T. & Hirschmann, M. M. Partial melting experiments of bimineralic eclogite and the role of recycled mafic oceanic crust in the genesis of ocean island basalts. *Earth Planet. Sci. Lett.* 249, 188–199 (2006).
- Dasgupta, R., Hirschmann, M. M. & Stalker, K. Immiscible transition from carbonate-rich to silicate-rich melts in the 3 GPa melting interval of eclogite + CO<sub>2</sub> and genesis of silica-undersaturated ocean island lavas. *J. Petrol.* 47, 647–671 (2006).
- Saal, A. E., Hart, S. R., Shimizu, N., Hauri, E. H. & Layne, G. D. Pb isotopic variability in melt inclusions from oceanic island basalts, polynesia. *Science* 282, 1481–1484 (1998).
- Novella, D. et al. The distribution of H<sub>2</sub>O between silicate melt and nominally anhydrous peridotite and the onset of hydrous melting in the deep upper mantle. Earth Planet. Sci. Lett. 400, 1–13 (2014).
- O'Leary, J. A., Gaetani, G. A. & Hauri, E. H. The effect of tetrahedral Al<sup>3+</sup> on the partitioning of water between clinopyroxene and silicate melt. *Earth Planet. Sci. Lett.* 297, 111–120 (2010).
- Hauri, E. SIMS analysis of volatiles in silicate glasses, 2: isotopes and abundances in Hawaiian melt inclusions. *Chem. Geol.* 183, 115–141 (2002)
- Dixon, J. E., Leist, L., Langmuir, C. & Schilling, J.-G. Recycled dehydrated lithosphere observed in plume-influenced mid-ocean-ridge basalt. *Nature* 420, 385–389 (2002).
- Castillo, P. R. A proposed new approach and unified solution to old Pb paradoxes. Lithos 252-253, 32-40 (2016).
- Chauvel, C., Hofmann, A. W. & Vidal, P. HIMU-EM: The French Polynesian connection. Earth Planet. Sci. Lett. 110, 99–119 (1992).
- Whalen, L. et al. Supercontinental inheritance and its influence on supercontinental breakup: the Central Atlantic Magmatic Province and the breakup of Pangea. Geochem. Geophys. Geosyst. 16, 3532–3554 (2015).
- Sheng, J., Liao, J. & Gerya, T. Numerical modeling of deep oceanic slab dehydration: implications for the possible origin of far field intra-contental volcanoes in northeastern China. J. Asian Earth Sci. 117, 328–336 (2016).
- Ryan, W. B. F. et al. Global Multi-resolution Topography synthesis. Geochem. Geophys. Geosyst. 10, Q03014 (2009).

Acknowledgements This study was supported by NSF OCE 1756349 and NSF EAR 1802012 to E.G. and NSF EAR-1249438 to E.A.J. The analytical work on EPMA facility in ISTerre, University Grenoble Alpes was supervised by V. Batanova and supported by grants of Institut Universitaire de France to A.V.S. and by the Richard Lounsbery Foundation to A.V.S. and E.G. S.E.M. thanks J. Dale, J. Trela, J. Berndt and L. Costello for help with sample collection, preparation and analyses. We are grateful to A. Hofmann for discussions. Any use of trade, product, or firm names is for descriptive purposes only and does not imply endorsement by the U.S. Government.



**Reviewer information** *Nature* thanks Gerya Taras and the other anonymous reviewer(s) for their contribution to the peer review of this work.

**Author contributions** S.E.M. prepared the samples, collected the bulk rock geochemistry data via X-ray fluorescence and laser ablation inductively coupled plasma–mass spectrometry, analysed data, wrote the paper and prepared figures and tables. E.G. conceived the project, analysed data and prepared figures. S.E.M., M.B. and P.B. performed the Pb, Sr, Nd and Hf isotopic analyses and P.B. conducted the Pb models. R.M. conducted the geodynamic models. E.A.J. performed the FTIR analyses of clinopyroxene. R.J.M. collected the  $^{40}$ Ar/ $^{39}$ Ar age dates. A.V.S. performed the electron microprobe analyses of olivine. All authors participated in the discussion and interpretations of results and in the preparation of the manuscript.

Competing interests The authors declare no competing interests.

#### **Additional information**

**Extended data** is available for this paper at https://doi.org/10.1038/s41586-019-1183-6.

**Supplementary information** is available for this paper at https://doi.org/10.1038/s41586-019-1183-6.

**Reprints and permissions information** is available at http://www.nature.com/reprints.

Correspondence and requests for materials should be addressed to S.E.M. or

**Publisher's note:** Springer Nature remains neutral with regard to jurisdictional claims in published maps and institutional affiliations.

© The Author(s), under exclusive licence to Springer Nature Limited 2019

## RESEARCH LETTER

#### **METHODS**

Selection of samples. Bermuda makes up only about 7% of the extinct shield volcano referred to as the Bermuda Pedestal, where the bulk of the volcanism occurred (Extended Data Fig. 1a). The pedestal and island are covered with Quaternary carbonates (Extended Data Fig. 1b), which range from calcareous dune deposits—formed when the platform was exposed during the Pleistocene glaciations—to coral limestones<sup>36</sup>. The platform is estimated to sit on top of oceanic crust that is 123—124 Myr old. We collected and analysed 40 samples from the Deep Drill 1972 Bermuda Core, which recovered 767 m of continuous igneous basement rock and is stored at Dalhousie University<sup>37</sup>. Samples were collected on average at 60-foot intervals (approximately 18.3 m), and are named by the depth in the core in feet to keep consistent with the original core log, that is, sample B703 corresponds to a depth of 703 feet. Below the carbonate cover, the borehole records alternating silica-undersaturated and silica-saturated volcanic units.

Bulk rock sample preparation. Samples were prepared for whole-rock analysis following the protocols in ref. <sup>38</sup>. Alteration-free rock chips of sample matrices were selected under a stereoscope microscope, powdered in an alumina mill, and fluxed into homogeneous glass disks with ultrapure 34.83% Li<sub>2</sub>B<sub>4</sub>O<sub>7</sub>-64.67% LiBO<sub>2</sub>−0.5% LiBr flux from Spex (certified ≪1 p.p.m. blank for all trace elements) in the Petrology Laboratory at Virginia Tech for X-ray fluorescence (XRF) and laser ablation inductively coupled plasma-mass spectrometry (LA-ICP-MS) analyses. Major element geochemistry was collected on a Panalytical EDS-XRF (EDS, energy-dispersive X-ray spectroscopy) with a silicon detector at the Department of Geosciences at Virginia Tech. The accuracy for USGS standard BHVO-2 (run as an unknown) was better than 2.5% for most major elements except Na<sub>2</sub>O (6.8%) and P<sub>2</sub>O<sub>5</sub> (3.3%), within reported values. The average relative standard deviation for 5 replicates of BHVO-2 were <1% for all major elements except Na<sub>2</sub>O and P<sub>2</sub>O<sub>5</sub> (both <3%). Trace elements from fluxed glasses were collected with an Agilent 7500ce ICPMS coupled with a Geolas laser ablation system following the procedures detailed in refs <sup>39,40</sup>, with a helium flow rate of approximately 1 l m<sup>-1</sup> at 5 Hz and an energy density per on sample of 7–10 J cm<sup>-2</sup>. LA-ICP-MS data was calibrated with fluxed glasses of USGS standards BHVO-2, BCR-2, BIR-1, and STM-1 using Ti from XRF as an internal standard. High-precision trace element standard values are from refs 39,41,42. The average relative accuracy for 5 replicates of BHVO-2 (run as an unknown) was better than 5% for most trace elements except Ge, Tm, Yb, Lu, and Pb (better than 15%). The average precision for BHVO-2 was better than 5% for all elements except V, Zn, Ge, Rb, Y, La and Th (<15%) (a complete statistical analysis is reported in Supplementary Table 2). **Extended geochemistry discussion.** The silica-saturated units range from basalt to basaltic trachyandesite (Fig. 2), and show higher degrees of alteration than the silica-undersaturated units, typically as calcite and haematite veins (Extended Data Fig. 2a). Near the base of the core there are interpreted pillow structures. The silica-undersaturated units range from foidite to basanite (Fig. 2) and are either porphyritic (Extended Data Fig. 2b) or aphanitic (Extended Data Fig. 2d), with minor alteration typically as calcite veins. In the porphyritic units, clinopyroxene is the most abundant phenocryst type, ranging from 1 mm to greater than 1 cm in size (Extended Data Fig. 2c, e). Zeolite species are also present in some of the silica-undersaturated units, and most of the olivine has been replaced by calcite (both zeolites and calcite were avoided during sample preparation). Two different mineralogical compositions were observed in the porphyritic silica-undersaturated units: the most common was clinopyroxene + nepheline + Ti-spinel  $\pm$  phlogopite  $\pm$  apatite  $\pm$  perovskite (Extended Data Fig. 2e, f), and the second grouping contained olivine + clinopyroxene + plagioclase + spinel. Where olivine is preserved it is fresh, with no alteration (Extended Data Fig. 2g) with fosterite content ranging from 84.7 to 88.8 wt%. Phlogopite has a Mg# (Mg# = Mg/(Mg + Fe)  $\times$ 100%) of 61.5, and up to 5.91 wt% TiO<sub>2</sub>.

Trace-element analyses confirm the visual interpretation that the silicaundersaturated units are minimally altered, with a general lack of enrichment (positive anomalies in the multi-element diagram, Fig. 2b) in Ba and Sr<sup>43</sup>. The silica-saturated units show positive Sr enrichments, which is probably a plagioclase signature, which agrees with the mineralogy that these silica-saturated units are plagioclase-normative, as opposed to the silica-undersaturated units being nepheline-normative. The silica-undersaturated and silica-saturated units differ considerably in their trace element compositions, with the silica-undersaturated units being generally more enriched than other Atlantic hotspots (including the Canaries, Cape Verde, St Helena, the Azores, Fernado de Noronha, and Madeira) and other ocean island basalts globally (Extended Data Fig. 4). The silica-undersaturated units are also characterized by a steep slope in the heavy rare earth elements (HREE) (Fig. 2b), and Gb/Yb ratios of between 3.3 and 6.0, indicating garnet fractionation in the source material<sup>44</sup>. The silica-saturated units are characterized by a flat HREE pattern and low (1.2-1.7) Gd/Yb ratios, indicating a shallower source region.

**Olivine geochemistry protocols.** High-precision olivine phenocryst analyses for Bermuda were conducted on the most primitive samples, following the

methods in ref. <sup>45</sup>. Data were collected at Institute Science de la Terrre (ISTerre) of the University Grenoble Alpes, Grenoble, France on a JEOL JXA-8230 Superprobe using a focused beam (approximately 1  $\mu m$  in diameter) of 25 kV and 900 nA. We analysed the San Carlos olivine standard at regular intervals during each analysis to correct for instrumental drift. Primary standards, statistics for the secondary standards, and statistics for the olivine analyses are given in Supplementary Table 2. Average approximate relative  $2\sigma$  errors for major and trace elements on the San Carlos olivine standard (n=33) were: Si, 0.16; Mg, 0.20; Fe, 0.029; Ni, 0.003; Mn, 0.001; Ca, 0.002; Na, 0.002; Al, 0.002; Co, 0.001; P, 0.001 and Ti, 0.001. An internal house standard (xen-7) was measured at regular intervals to correct for instrumental drift in Zn. The  $2\sigma$  error for Zn on xen-7 was ~0.001. The relative accuracy for San Carlos olivine standard was better than 1% for all oxides.

Silica-undersaturated melts: insights from experiments. The trace-element and isotopic characteristics of silica-undersaturated, alkaline magmas cannot be explained by simple peridotite melting. For example, CaO and TiO<sub>2</sub> contents of alkaline basalts are higher than in tholeiitic basalts and cannot be the product of melting primitive mantle alone<sup>46</sup>. As a result, experimental studies over the past two decades have attempted to constrain the relationship between silica-undersaturated magmas and their possible source rocks. These experiments have investigated the melting of various enriched rock types to produce silica-undersaturated, alkaline magmas: carbonated peridotite<sup>22,23,47</sup>, carbonated eclogite<sup>48,49</sup>, eclogite/garnet pyroxenite<sup>24</sup>, and hornblendite/clinopyroxene bearing hornblendite<sup>50</sup>.

These experiments have increased our understanding of the recycling of volatile and trace element enriched rock types. Low-degree melts from carbonated peridotite between 2–5 GPa and 1,350–1,600 °C produce silica-undersaturated melts that are high in  $\text{CaO}^{22}$  (Extended Data Fig. 5) with the solidus starting 150 °C lower than  $\text{CO}_2$ -free peridotite. The experimental melts are within the range of those found in Bermuda but fail to account for  $K_2\text{O}$  and  $\text{Al}_2\text{O}_3$  contents (Extended Data Fig. 5). The solidus for carbonated eclogite is steeper than for carbonated peridotite, and can also account for the high CaO contents of alkaline intraplate magmatism  $^{48}$ . However, the carbonated eclogite experiments cannot account for the range of TiO $_2$  exhibited by Bermuda (Extended Data Fig. 5).

Experiments using hornblendite and clinopyroxene-bearing hornblendite represent the melting of hydrous metasomatic veins  $^{50}$ . These results (run at 1.5 GPa) suggest that the metasomatized lithosphere is recycled by subduction or delamination and melts to produce silica-undersaturated alkaline magmas. Silica-undersaturated lavas from Bermuda overlap with the experimental melts of a clinopyroxene-bearing hornblendite, with good agreement in  $\rm TiO_2$ ,  $\rm CaO$ ,  $\rm Al_2O_3$  and  $\rm K_2O$  with  $\rm SiO_2$  abundances (Extended Data Fig. 5). Although the experimental melting of hornblendite can explain the low  $\rm SiO_2$  in correlation with several major elements, melting of hornblende/clinopyroxene rich samples cannot account for the low Ni content measured in the Bermuda olivine.

When comparing the Bermuda silica-undersaturated lavas with experimental studies, we can conclude that simple melting of carbonated peridotite cannot account all for the major element compositions of the lavas. Similar results were found for the silica-undersaturated, alkaline lavas from St Helena<sup>51</sup> (the Atlantic HIMU end member), as carbonated peridotite alone cannot account for the composition of St Helena and thus they invoke an additional component of subducted oceanic crust.

Lamporites from the Leucite Hills (WY) are thought to be representative of melting carbonated metasomatic veins that are composed of phlogopite  $\pm$  richterite  $\pm$  clinopyroxene  $\pm$  apatite  $\pm$  titanite  $^{52}$ . Bermuda silica-undersaturated mineralogy shares this characteristic metasomatic mineralogy, further supporting melting of metasomatized domains within the mantle. Additionally, Bermuda silica-undersaturated lavas have increased Nb/U ratios (up to 66) compared with canonical mantle values (approximately 52), which is an additional indicator for (carbonatite) metasomatism  $^{53}$ . Combined with bulk rock trace element compositions, olivine compositions (discussed in main text), and magmatic water calculations (discussed below), we suggest that Bermuda is the product of melts of volatile (H2O and CO2) enriched garnet peridotite.

Magmatic water from clinopyroxenes. Polarized infrared spectra of the hydroxy (OH) group in clinopyroxene were collected at  $4\text{-cm}^{-1}$  resolution using a  $180 \times 180 \,\mu\text{m}$  spot size via a Nic-Plan microscope attachment on the Thermo-Nicolet Magna 750 Fourier transform infrared (FTIR) spectrometer at James Madison University, with a KBr beamsplitter and a wire grid polarizer, and averaging over 256 scans. Each pyroxene crystal was made into a four-sided rectangular prism, with sides polished to a smooth finish using 1 μm grit alumina or diamond paper. This enabled three mutually perpendicular infrared spectra to be obtained on the same crystal for quantification  $^{54}$ . The clinopyroxenes are black to dark brown, precluding the use of interference figures to determine crystallographic orientation. OH concentrations of the clinopyroxene phenocrysts were calculated using the total integrated OH band areas between 3,700 and 3,000 cm $^{-1}$ , and using the modified Beer–Lambert law and the integral specific absorption coefficient (I') for clinopyroxene from ref.  $^{55}$ . Major elements of the same clinopyroxenes used

for FTIR analysis were conducted at the University of Münster in the Institute for Mineralogy on a JEOL JXA 8900 electron microprobe using a focused beam of 15 kV, 100 nA, and a beam diameter of 10  $\mu m$ . Other mineral phases in the silica-undersaturated unit were analysed at Virginia Tech with a Cameca SX 50 electron microprobe using a focused beam of 15 kV, 25nA, and a beam diameter of 1  $\mu m$ .

The clinopyroxenes from Bermuda silica-undersaturated lavas have  $H_2O$  concentrations that range from 314 to 694 p.p.m.  $H_2O$  (wt%). The two samples from the upper part of the core (B322, B830) have on average the lowest  $H_2O$  concentrations, 393  $\pm$  54 and 395  $\pm$  52 p.p.m., respectively (Supplementary Table 2). The middle to lower sections of the core have higher  $H_2O$  concentrations, averaging from 574  $\pm$  94 (B1445), 637  $\pm$  91 (B1644) and 629  $\pm$  14 p.p.m. (B2299). Magmatic water concentrations for clinopyroxene-bearing lavas are calculated on the basis of experimental partition coefficient ( $D_{H_2O}^{\rm Cpx/Mell}$ ) data, which positively corresponds to increasing Al contents in the clinopyroxenes. We used the  $D_{H_2O}^{\rm Cpx/Mell}$  calculations of refs  $^{27,28}$ . Equation 10 of ref.  $^{28}$  is as follows:

$$D_{\rm H,O}^{\rm Cpx/Melt} = e^{-4.2(\pm 0.2) + 6.5(\pm 0.5)X_{\rm VAI}^{\rm Cpx} - 1.0(\pm 0.2)X_{\rm Ca}^{\rm Cpx}}$$

Whereas the relevant equation in ref. <sup>27</sup> is expressed as:

$$D_{\text{H}_2\text{O}}^{\text{Cpx/melt}} = 0.0016 \times \text{Al}_2\text{O}_3 \text{(wt\%)} + 0.0078$$

The  $D_{\rm H_2O}^{\rm Cpx/Melt}$  calculation of ref.  $^{28}$  uses the relationship of tetrahedrally coordinated Al $^{3+}$  (l $^{\rm V}$ Al $^{3+}$ ) and Ca in the clinopyroxenes, whereas ref.  $^{27}$  uses the Al $_2O_3$  content. Al $_2O_3$  content ranges between 3.72 and 8.58 wt%, with B322 having the lowest Al $_2O_3$  and  $^{\rm IV}$ Al $^{3+}$  concentrations (average 4.16  $\pm$  0.44 wt% and 0.081  $\pm$  0.010, respectively), while the other samples have higher concentrations (>5.37 wt% Al $_2O_3$  and >0.103  $^{\rm IV}$ Al $^{3+}$ ). The  $D_{\rm H_2O}^{\rm Cpx/Melt}$  calculated from ref.  $^{28}$  yields higher H $_2O_{(1)}$  concentrations with larger errors (ranging from 2.57  $\pm$  0.78 to 5.75  $\pm$  1.71 wt%), but on average they are still within error of the H $_2O_{(1)}$  concentrations calculated in ref.  $^{27}$  (ranging between 1.87  $\pm$  0.18 to 4.07  $\pm$  0.39 wt%).

Intraplate volcanoes typically have a low magmatic  $\rm H_2O$  content of between 0.03 and 1 wt%  $\rm H_2O$ , whereas are volcanoes average 4 wt%  $\rm H_2O^{56}$ . Our calculations show that the silica-undersaturated lavas from Bermuda have  $\rm H_2O$  contents that are greater than those of other typical intraplate volcanoes, approaching the high  $\rm H_2O$  contents of arc volcanics. Therefore, Bermuda must have sampled a mantle domain that was rich in volatiles, an observation that agrees with major element compositions (discussed above).

Radiogenic isotope protocols. Radiogenic isotope ratios were determined at the Center for Elemental Mass Spectrometry (CEMS), University of South Carolina (USC) following the established procedure for this laboratory<sup>57,58</sup>. Sample powders from the same aliquots used for major and trace elements were digested in a sub-boiling Teflon-distilled 3:1 HF:HNO3 mixture, and the isotopes were analysed from aliquots of a single digestion. Pb was separated on an anion resin with HBr and HNO<sub>3</sub>. Replicate Pb analyses were conducted on four of the most radiogenic <sup>206</sup>Pb/<sup>204</sup>Pb samples (sample numbers B703, B1644, B1873, and B1908) by leaching the powders for 2 h in 6 M HCl to account for any clinopyroxene signal bias. Sr and rare-earth elements were separated from the bulk-rock washes of the Pb chemistry on a cation resin in HCl. Sr was further purified on a Sr-spec resin and Nd on an Ln-resin. Hf cuts from the Pb washouts were processed with Ln-spec resin (Eichrom) following the procedures in ref. <sup>59</sup>. Isotopic ratios for Pb, Nd, Hf, and Sr were obtained on a Neptune multicollector ICP-MS at USC. Samples were introduced with an APEX enhanced sensitivity spray chamber and high-sensitivity cones (JET and X-skimmer configuration).

Pb isotope ratios were determined by the Tl-addition technique  $^{60}$  using the fractionation correction and data-reduction method outlined in ref.  $^{61}$ . The method calculates an empirical exponential mass fractionation factor based on the relative Pb and Tl isotope fractionation of NBS-981 Pb standard that was run multiple times with the samples and forcing the standard to a reference value, for which we used the values proposed in ref.  $^{62}$ .  $^{206}\text{Pb}/^{204}\text{Pb} = 16.9405$ ,  $^{207}\text{Pb}/^{204}\text{Pb} = 15.4963$ , and  $^{208}\text{Pb}/^{204}\text{Pb}$  36.7219. The Pb/Tl ratio ( $^{208}\text{Pb}/^{205}\text{Tl} \approx 7$ ) of the samples was kept almost identical to the NBS 981 standard by first performing dip checks in the samples and spiking Tl to the appropriate level. The reproducibility of the method was judged by the repeated analyses of NBS-981 within the analytical session  $^{206}\text{Pb}/^{204}\text{Pb} = 0.0012$ , and  $^{208}\text{Pb}/^{204}\text{Pb} = 0.004$  (2 $\sigma$ , n=19). The USGS AGV-2 standard was measured in the same analytical sequence as most of the samples reported here and is within error of recommended values  $^{63}$  (Extended Data Fig. 8).

The Nd standard JNdi was measured at  $^{143}$ Nd/ $^{144}$ Nd = 0.512097  $\pm$  0.000016 ( $2\sigma$ , n=11) at USC, and the values are reported relative to the accepted value of JNdi of  $^{143}$ Nd/ $^{144}$ Nd = 0.512115. Isotopic ratios for Nd were normalized to  $^{146}$ Nd/ $^{144}$ Nd = 0.7219.  $^{176}$ Hf/ $^{177}$ Hf ratios were corrected for mass fractionation using  $^{179}$ Hf/ $^{177}$ Hf = 0.7325, and the accuracy of analyses was monitored by

repeated measurements of the JMC-475 standard<sup>64</sup>, which gave an average value of  $^{176} \rm Hf/^{177} \rm Hf = 0.282144 \pm 0.000005 \, (2\sigma, n=10)$ . The isotope ratios are reported relative to the generally accepted value  $^{176} \rm Hf/^{177} \rm Hf = 0.282160$ .  $\varepsilon \rm Nd$  and  $\varepsilon \rm Hf$  are the deviations (in parts per ten thousand) from chondritic values of 0.512638 for  $^{143} \rm Nd/^{144} \rm Nd$  and 0.282772 for  $^{176} \rm Hf/^{177} \rm Hf$ . Isotopic ratios for Sr were normalized to  $^{86} \rm Sr/^{88} \rm Sr = 0.1194$ , and replicate analyses of standard NBS-987 yielded  $^{87} \rm Sr/^{86} \rm Sr = 0.710316 \pm 0.000013 \, (2\sigma, n=7)$ . All Sr measurements are reported relative to NBS-987  $^{87} \rm Sr/^{86} \rm Sr = 0.710250$ . USGS standards BCR-2 and BHVO-1 were run as unknowns and are presented in Supplementary Table 2. Full procedural blanks were run at Pb < 38 pg, Sr < 80 pg, Nd < 10 pg and Hf < 60 pg.

Lead isotopes modelling: evaluating the possibility that the Bermuda lavas form an isochron. The slope of the silica-undersaturated lavas samples (Extended Data Fig. 6a) corrected for 30 Myr ago in  $^{206}\text{Pb}/^{204}\text{Pb}-^{207}\text{Pb}/^{204}\text{Pb}$  space corresponds to an age  $t_1$  given the following equation:

slope = 
$$\frac{1}{137.88} \times \frac{e^{\lambda_{235} \times t_1} - e^{\lambda_{235} \times t_2}}{e^{\lambda_{238} \times t_1} - e^{\lambda_{238} \times t_2}}$$

where  $t_2 = 30$  Myr and  $\lambda_{235}$  and  $\lambda_{238}$  are the decay constants for  $^{235}$ U and  $^{238}$ U, respectively, with  $\lambda_{235} = 9.849 \times 10^{-10} \, \text{yr}^{-1}$  and  $\lambda_{238} = 1.551 \times 10^{-10} \, \text{yr}^{-1}$ .

The calculated slope (linear regression through age-corrected data) has a value of 0.0459 with a  $2\sigma$  error of  $\pm 0.0009$ . This corresponds to a  $t_1$  value of  $-36.4 \pm 97.7$  Myr, which means that most of the corresponding age range is in the future. The maximum age possible (95% confidence) is 55.9 Myr, 25.9 Myr before lava eruption at 30 Myr ago.

The silica-undersaturated samples are therefore unlikely to form an isochron, but if this is the case, this isochron has a near-zero age (<25.9 Myr before eruption of lavas); in addition, an unrealistically high  $\mu$  value ( $^{238}$ U/ $^{204}$ Pb >400) would be required to explain the most radiogenic sample from an initial isotope value similar to that of the least radiogenic one.

If we consider all of the Bermuda lavas as coming from the same Pb source, we can apply the same logic presented above to attempt to calculate a second isochron. The calculated slope of all the Bermuda samples corrected for 30 Myr ago in  $^{206}\text{Pb}/^{204}\text{Pb}-^{207}\text{Pb}/^{204}\text{Pb}$  is 0.0468 with a  $2\sigma$  error of  $\pm 0.0009$ . This corresponds to a  $t_1$  value of 40 Myr and still requires unrealistically high  $\mu$  values.

Lead isotope modelling: evaluating the possibility that the silica-undersaturated Bermuda lavas form a mixing line. Another way to explain the trend formed by the silica-undersaturated lavas is mixing between a moderately depleted source similar to the Bermuda silica-saturated units and a highly radiogenic end member  $(^{206}\text{Pb}/^{204}\text{Pb} > 21.5;$  Extended Data Fig. 6a).

We can therefore model how to produce a mixing end member with the isotopic composition of the most radiogenic sample (B703). The mixing end member of the silica-undersaturated lavas group is probably more radiogenic (further away from the data on the mixing line); however, sample B703 can be used to calculate the minimum  $\mu = ^{238}\text{U}/^{204}\text{Pb}$  value for any possible mixing end member, because  $\mu \propto R_2 - R_1$  in a scenario in which a source with a  $^{206}\text{Pb}/^{204}\text{Pb}$  ratio  $R_1$  evolves over time to a ratio  $R_2$  with a given value of  $\mu$ . Also, the slope of an isochron tying a given  $R_1$  value in  $^{206}\text{Pb}/^{204}\text{Pb}-^{207}\text{Pb}/^{204}\text{Pb}$  space with a point  $R_2$  will become shallower the higher the  $^{206}\text{Pb}/^{204}\text{Pb}$  value of  $R_2$ , yielding a younger age, and therefore requiring a higher  $\mu$ .

We calculate the  $\mu$  required to generate a component with the isotopic composition of B703 using the following equation:

$$\mu = \frac{R_2 - R_1}{e^{\lambda_{238} \times t_1} - e^{\lambda_{238} \times t_2}} \tag{1}$$

where  $R_2$  is the  $^{206}\text{Pb}/^{204}\text{Pb}$  ratio of sample B703 corrected for an eruption age  $t_2 = 30$  Myr, and  $R_1$  is the  $^{206}\text{Pb}/^{204}\text{Pb}$  ratio of a mantle source at  $t_1$  (fractionation

Because the least radiogenic <sup>206</sup>Pb/<sup>204</sup>Pb Bermuda samples (the silica-saturated lavas) have a similar Pb isotopic signature as the composition of the Mid-Atlantic Ridge (MAR) near the Azores, we assume that the least radiogenic Bermuda samples plot along the Atlantic Array. This assumption ties Bermuda silica-saturated samples with the Azores MAR, Average NMAR, and Iceland MAR (Extended Data Fig. 6a, b), with a minimum <sup>206</sup>Pb/<sup>204</sup>Pb ratio of 18 (see Atlantic MORB data in ref. <sup>65</sup>)

All modelled isochrons intersect at point  $R_2$  in the  $^{206}\text{Pb}/^{204}\text{Pb}-^{207}\text{Pb}/^{204}\text{Pb}$  space and plot below the trend of the silica-undersaturated lavas, as it equates a near-zero isochron. The shallowest modelled isochron therefore corresponds to the unlikely scenario in which the silica-undersaturated lavas form an isochron instead of a mixing line.

With the constraint of a point  $R_1$  on the Atlantic array, every value of  $R_1$  ( $^{206}\text{Pb}/^{204}\text{Pb}, ^{207}\text{Pb}/^{204}\text{Pb}$ ) will correspond to a single  $t_1$  value (unique slope) and  $\mu$ . The Atlantic array corresponds to  $R_1$  values at  $t_3$  (today). We therefore calculate  $R_1$  at  $t_1$  before using equation (1), assuming a  $\mu$  value of 8 for the mantle.



Given the transcendental nature of equation (1), we use a Monte Carlo approach to constrain what combinations of  $t_1$  and  $\mu$  correspond to  $R_1$  values on the Atlantic array  $(R_1^{\frac{307}{Pb}})^{\frac{304}{Pb}} = 0.1328 \times R_1^{\frac{306}{Pb}})^{\frac{304}{Pb}} + 13.0325 \pm 0.002)$ . We further calculate the  $\Omega = \frac{232}{Pb}$ Th/ $\frac{204}{Pb}$  values required to reach the

We further calculate the  $\Omega^{\frac{-2}{2}}$  <sup>232</sup>Th/<sup>204</sup>Pb values required to reach the <sup>208</sup>Pb/<sup>204</sup>Pb value of the most radiogenic Bermuda sample (B703) from the  $R_1^{\frac{208}{10}}$  on the Atlantic array corresponding to each valid simulation, assuming an  $\Omega$  value of 24 for the mantle. Finally, we calculate the  $\kappa = ^{232}$ Th/<sup>238</sup>U =  $\Omega/\mu$  values corresponding to modelled  $\mu$  and  $\Omega$ .

Results are reported in Supplementary Table 3 and Extended Data Fig. 6c–f.  $\mu$  and  $\Omega$  increase exponentially with  $R_1$  and  $t_1$ . Any  $R_1$  value more radiogenic than average NMAR yields ages younger than 650 Myr,  $\mu>35$  and  $\Omega>100$ , which again are minimum parent/daughter values for this mixing scenario.  $R_1$  values in the vicinity of Bermuda silica-saturated lavas (both isochron and mixing scenarios possible) yield ages around 200 Myr and extreme  $\mu$  values over 100, and  $\Omega$  greater than 250. By contrast, modelled  $\kappa$  values range from 2.6 to 2.9, which correspond to Phanerozoic mantle values modelled in ref.  $^{66}$ .

 $^{40}\text{Ar}/^{39}\text{Ar}$  geochronology. In samples B1641 and B1908, large (around 1 mm) phenocrysts were selected from gently ground gravels. For samples B703 and B1036, smaller (around 150–300  $\mu\text{m}$ ) phenocrysts of biotite were separated by crushing, grinding, magnetic separation and extensive handpicking. The biotite separates for  $^{40}\text{Ar}/^{39}\text{Ar}$  dating were loaded in high-purity copper foil and irradiated in the central thimble of the USGS TRIGA reactor in Denver, Colorado, during two separate irradiations of 20 (KD62) and 30 megawatt hours (KD64), and all isotopic analyses were completed at the USGS-Reston  $^{40}\text{Ar}/^{39}\text{Ar}$  geochronology laboratory. Fish Canyon Tuff sanidine, with an astronomically tuned age of 28.201  $\pm$  0.08 Myr (ref.  $^{67}$ ), was used as the neutron fluence monitor in both irradiations. Values for interfering isotopes were determined by analysis of CaF2 glass and K2SO4 salt from irradiation KD62. These values were used for both KD62 and KD64. Production factors change little over time at the USGS-TRIGA reactor  $^{68}$ .

Following irradiation, unknown samples were heated in low-blank furnaces similar to that described in ref. <sup>69</sup>. The evolved gases were then purified in two-stage ultra-high vacuum extraction lines<sup>70</sup>, and analysed on either a Mass Analyzer Products 216 (sample B1908) or a VG Micromass 1200 (samples B703, B1036, B1641) noble gas mass spectrometer, both operating in static mode. The Ar isotopes were measured by peak hopping using a SEV217 electron multiplier on the VG1200 and a Johnston MM1 electron multiplier on the MAP216. Isotopes were measured in six cycles and the time-zero intercepts were determined by linear regressions of the data.

Data from the VG1200 were reduced using a modified version of ArAr\* (ref.  $^{71}$ ) and MassSpec V. 7.9 (ref.  $^{72}$ ) and Isoplot  $^{73}$  was used to reduce data from the MAP216. In each program, a plateau age was defined as a set of contiguous steps containing more than 60% of the  $^{39}{\rm Ar_{K}}$ , where the probability of fit of the weighted mean age of the steps is greater than 5% (ref.  $^{74}$ ). To maintain consistency with ref.  $^{67}$  (Fish Canyon Tuff sanidine age of 28.201  $\pm$  0.08 Myr), the decay constants from ref.  $^{74}$  and the Ar isotopic composition from ref.  $^{75}$  were used in data reduction. Constants and complete isotopic data can be found in the data tables in Supplementary Table 1.

We were unable to successfully date the matrix from the silica-saturated units, but phlogopite separates from the silica-undersaturated units B703, B1641 and B1908 yield  $^{40} \rm Ar/^{39} Ar$  plateau ages of 30.89  $\pm$  0.21, 30.917  $\pm$  0.096 and 30.89  $\pm$  0.26 Myr, respectively (Extended Data Fig. 3). All ages are at  $2\sigma$  and include the error in the irradiation parameter *J*. These ages are interpreted to represent the time of crystallization of these silica-undersaturated lavas and, within limits of error, document contemporaneous emplacement of these units. Step-heating of sample B1908 yielded a slightly more complex age spectrum, and ages with more than 2% of the  $^{39} \rm Ar_K$  vary between 34.37 and 35.04 Myr, yielding a preferred age of 34.61  $\pm$  0.87 (2 $\sigma$  error expanded by  $\sqrt{\rm MSWD}$  (mean square weighted deviation)). We interpret this age to document a discrete pulse of magmatism approximately 4 Myr before that recorded in the other samples. We cannot unequivocally rule out excess Ar as a cause for the older age, but the biotite appears unaltered under incident light and we see no reason to invoke excess Ar.

A model for Bermuda. In addition to the unique isotopic signatures recorded in the silica-undersaturated units of Bermuda, the alternating silica-undersaturated and silica-saturated composition is another feature that renders Bermuda an important location from which to understand the geochemical evolution of the mantle. As discussed above, the silica-saturated units fall within the Atlantic Array in terms of <sup>206</sup>Pb/<sup>204</sup>Pb, <sup>207</sup>Pb/<sup>204</sup>Pb and <sup>208</sup>Pb/<sup>204</sup>Pb. <sup>143</sup>Nd/<sup>144</sup>Nd and <sup>176</sup>Hf/<sup>177</sup>Hf approach the depleted mantle reservoir, but <sup>87</sup>Sr/<sup>86</sup>Sr is more radiogenic than is depleted mantle and is similar to values from the silica-undersaturated units. Trace-element signatures, particularly those of the heavy rare-earth elements, from the silica-saturated units suggest that that these melts were derived from a shallower source region where garnet was not stable. Together, the radiogenic isotopes and geochemical composition of the silica-saturated units suggest that they were derived from a depleted, shallow upper mantle similar to the source of MORB.

Geochemical data support a deep-seated reservoir rich in volatiles, and when coupled with our geodynamic models, we can suggest that Bermuda silica-undersaturated melts are the product of a small convection cell that sampled the volatile-rich transition zone. The transition zone was enriched with young recycled material evident from Pb isotopes, probably stored in the transition zone either owing to subduction associated with the coalescence of Pangea or delamination of crustal material during the subsequent break-up of Pangea. That volatile-rich material melted in the transition zone owing to the convection cell (Fig. 1). The volatile-rich melt interacted with peridotites above the transition zone, generating the silica-undersaturated melts (Fig. 1). The convecting cell is also responsible for melting the already depleted upper mantle, triggering shallow silica-saturated melts that are interlayered with the silica-undersaturated melts. The advection of global mantle flow backwards in time for our geodynamic modelling was conducted following the procedures outlined in ref. <sup>76</sup>. The recycled material in the transition zone in our schematic model (Fig. 1) follows the modelling in ref. <sup>77</sup>.

#### Data availability

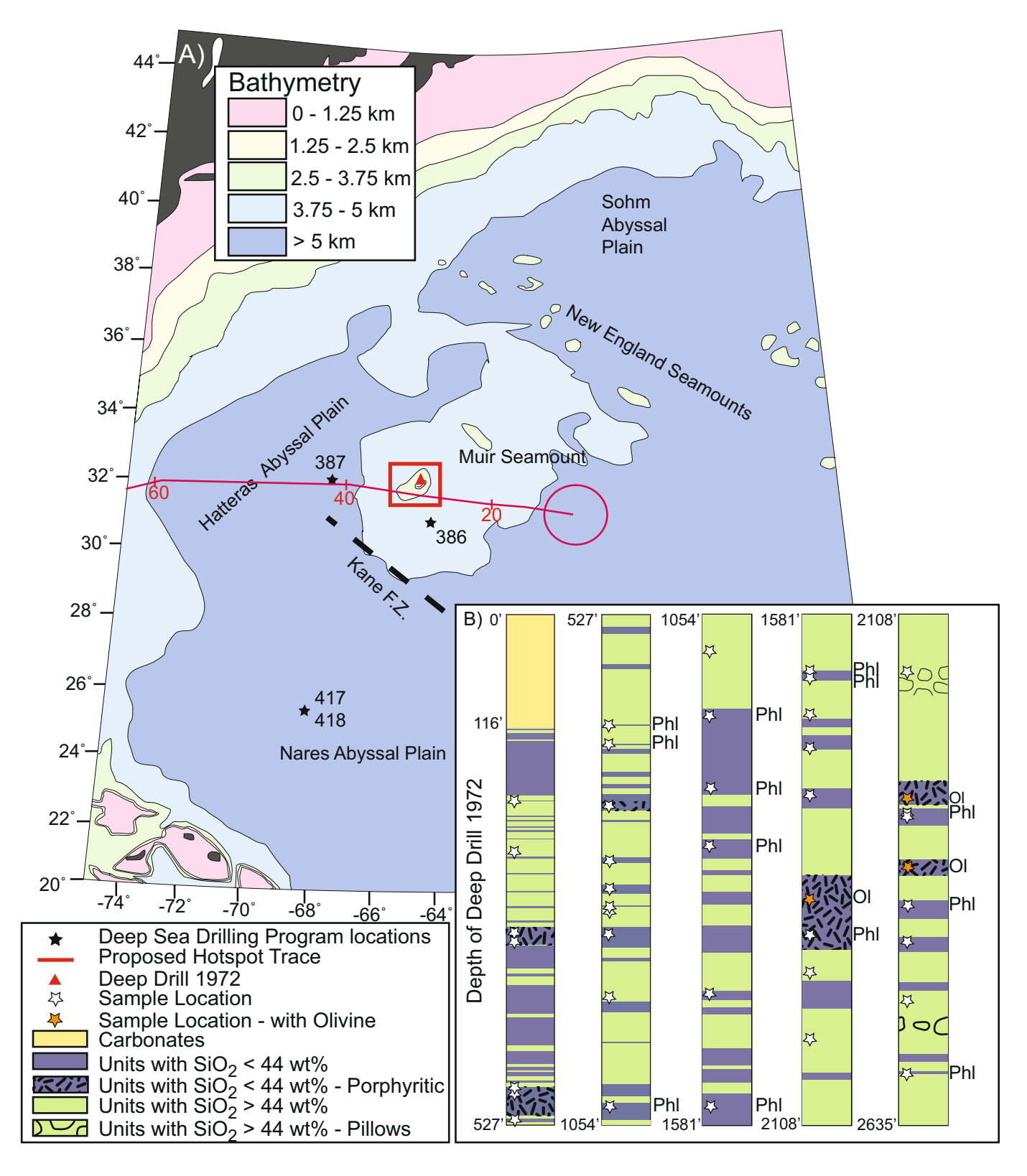
Geochemical data for Bermuda lavas can be found online at the EarthChem database at https://doi.org/10.1594/IEDA/111282. All geochemical data—including olivine-spinel thermometry, magmatic water calculations and Pb-isotope modelling—can be found in the Supplementary Information.

- Rowe, M. P. An Explanation of the Geology of Bermuda (Bermuda Government, Ministry of the Environment. 1998).
- Rice, P. D., Hall, J. M. & Opdyke, N. D. Deep Drill 1972: a paleomagnetic study of the Bermuda Seamount. Can. J. Earth Sci. 17, 232–243 (1980).
- Mazza, S. E. et al. Volcanoes of the passive margin: the youngest magmatic event in eastern North America. Geology 42, 483–486 (2014).
- Kelley, K. A., Plank, T., Ludden, J. & Staudigel, H. Composition of altered oceanic crust at ODP Sites 801 and 1149. Geochem. Geophys. Geosyst. 4, 8910 (2003).
- 40. Gazel, E. et al. Lithosphere versus asthenosphere mantle sources at the Big Pine Volcanic Field, California. Geochem. Geophys. Geosyst. 13, QOAK06 (2012).
- He, Y. et al. High-precision iron isotope analysis of geological reference materials by high-resolution MC-ICP-MS. Geostand. Geoanal. Res. 39, 341–356 (2015)
- Willbold, M. & Jochum, K. P. Multi-element isotope dilution sector field ICP-MS: a precise technique for the analysis of geological materials and its application to geological reference materials. Geostand. Geoanal. Res. 29, 63–82 (2005).
- Pearce, J. & Peate, D. Tectonic implications of the composition of volcanic arc magmas. Annu. Rev. Earth Planet. Sci. 23, 251–285 (1995).
- Johnson, K. T. Experimental determination of partition coefficients for rare earth and high-field-strength elements between clinopyroxene, garnet, and basaltic melt at high pressures. Contrib. Mineral. Petrol. 133, 60–68 (1998).
- Batanova, V. G., Sobolev, A. V. & Kuzmin, D. V. Trace element analysis of olivine: high precision analytical method for JEOL JXA-8230 electron probe microanalyser. Chem. Geol. 419, 149–157 (2015).
- Prytulak, J. & Elliott, T. TiO<sub>2</sub> enrichment in ocean island basalts. Earth Planet. Sci. Lett. 263, 388–403 (2007).
- Dasgupta, R. & Hirschmann, M. M. Melting in the Earth's deep upper mantle caused by carbon dioxide. *Nature* 440, 659–662 (2006).
- Dasgupta, R., Hirschmann, M. M. & Withers, A. C. Deep global cycling of carbon constrained by the solidus of anhydrous, carbonated eclogite under upper mantle conditions. *Earth Planet. Sci. Lett.* 227, 73–85 (2004).
  Dasgupta, R., Hirschmann, M. M. & Stalker, K. Immiscible transition from
- Dasgupta, R., Hirschmann, M. M. & Stalker, K. Immiscible transition from carbonate- rich to silicate-rich melts in the 3 GPa melting interval of eclogite + CO<sub>2</sub> and genesis of silica-undersaturated ocean island lavas. *J. Petrol.* 47, 647–671 (2006).
- Pilet, S., Baker, M. B. & Stolper, E. M. Metasomatized lithosphere and the origin of alkaline lavas. Science 320, 916–919 (2008).
- Kawabata, H. et al. The petrology and geochemistry of St. Helena alkali basalts: evaluation of the oceanic crust-recycling model for HIMU OIB. J. Petrol. 52, 791–838 (2011).
- Mirnejad, H. & Bell, K. Origin and source evolution of the Leucite Hills lamproites: evidence from Sr–Nd–Pb–O isotopic compositions. J. Petrol. 47, 2463–2489 (2006).
- Hofmann, A.W. in *Treatisese on Geochemistry* 2nd edn, Vol. 3 (eds Holland, H. D. & Turekian, K. K.) 67–101 (Elsevier, Oxford, 2014)
- 54. Johnson, E. A. & Rossman, G. R. A survey of hydrous species and concentrations in igneous feldspars. *Am. Min.* **89**, 586–600 (2004).
- 55. Rossman, G. R., Bell, D. R. & Ihinger, P. D. Quantitative analysis of trace OH in garnet and pyroxenes. *Am. Min.* **80**, 465–474 (1995).
- Plank, T., Kelley, K. A., Zimmer, M. M., Hauri, E. H. & Wallace, P. J. Why do mafic arc magmas contain ~4wt% water on average? Earth Planet. Sci. Lett. 364, 168–179 (2013).
- Bizimis, M., Salters, V. J., Garcia, M. O. & Norman, M. D. The composition and distribution of the rejuvenated component across the Hawaiian plume: Hf, Nd, Sr, Pb isotope systematics of Kaula lavas and pyroxenite xenoliths. Geochem. Geophys. Geosyst. 14, 4458–4478 (2013).
- Khanna, T. C., Bizimis, M., Yogodzinski, G. M. & Mallick, S. Hafnium–neodymium isotope systematics of the 2.7 Ga Gadwal greenstone terrane, Eastern Dharwar craton, India: implications for the evolution of the Archean depleted mantle. Geochim. Cosmochim. Acta 127, 10–24 (2014).



- Münker, C., Weyer, S., Scherer, E. & Mezger, K. Separation of high field strength elements (Nb, Ta, Zr, Hf) and Lu from rock samples for MC-ICPMS measurements. *Geochem. Geophys. Geosyst.* 2, 1064 (2001).
- White, W. M., Albarède, F. & Télouk, P. High-precision analysis of Pb isotope ratios by multi-collector ICP-MS. Chem. Geol. 167, 257–270 (2000).
- Todd, E., Stracke, A. & Scherer, E. E. Effects of simple acid leaching of crushed and powdered geological materials on high-precision Pb isotope analyses. Geochem. Geophys. Geosyst. 16, 2276–2302 (2015).
- Galer, S. J. G. & Abouchami, W. Practical application of lead triple spiking for correction of instrumental mass discrimination. *Mineral. Mag.* 62A, 491–492 (1998).
- Weis, D. et al. High-precision isotopic characterization of USGS reference materials by TIMS and MC-ICP-MS. Geochem. Geophys. Geosyst. 7, Q08006 (2006).
- Patchett, P. J. & Tatsumoto, M. A routine high-precision method for Lu-Hf isotope geochemistry and chronology. *Contrib. Mineral. Petrol.* 75, 263–267 (1981).
- Stracke, A. Earth's heterogeneous mantle: A product of convection-driven interaction between crust and mantle. Chem. Geol. 330–331, 274–299 (2012).
- Elliott, T., Zindler, A. & Bourdon, B. Exploring the kappa conundrum: the role of recycling in the lead isotope evolution of the mantle. Earth Planet. Sci. Lett. 169, 129–145 (1999).
- Kuiper, K. F. et al. Synchronizing rock clocks of Earth history. Science 320, 500–504 (2008).
- Snee, L. W. Argon Thermochronology of Mineral Deposits: A Review of Analytical Methods, Formulations, and Selected Applications. Bulletin 2194 (US Geological Survey, 2002).
- 69. Staudacher, T., Jessberger, E., Dorflinger, D. & Kiko, J. A refined ultrahigh-vacuum furnace for rare gas analysis. *J. Phys. E* **11**, 781 (1978).
- McAleer, R. et al. Reaction softening by dissolution–precipitation creep in a retrograde greenschist facies ductile shear zone, New Hampshire, USA. J. Metamorph. Geol. 35, 95–119 (2017).

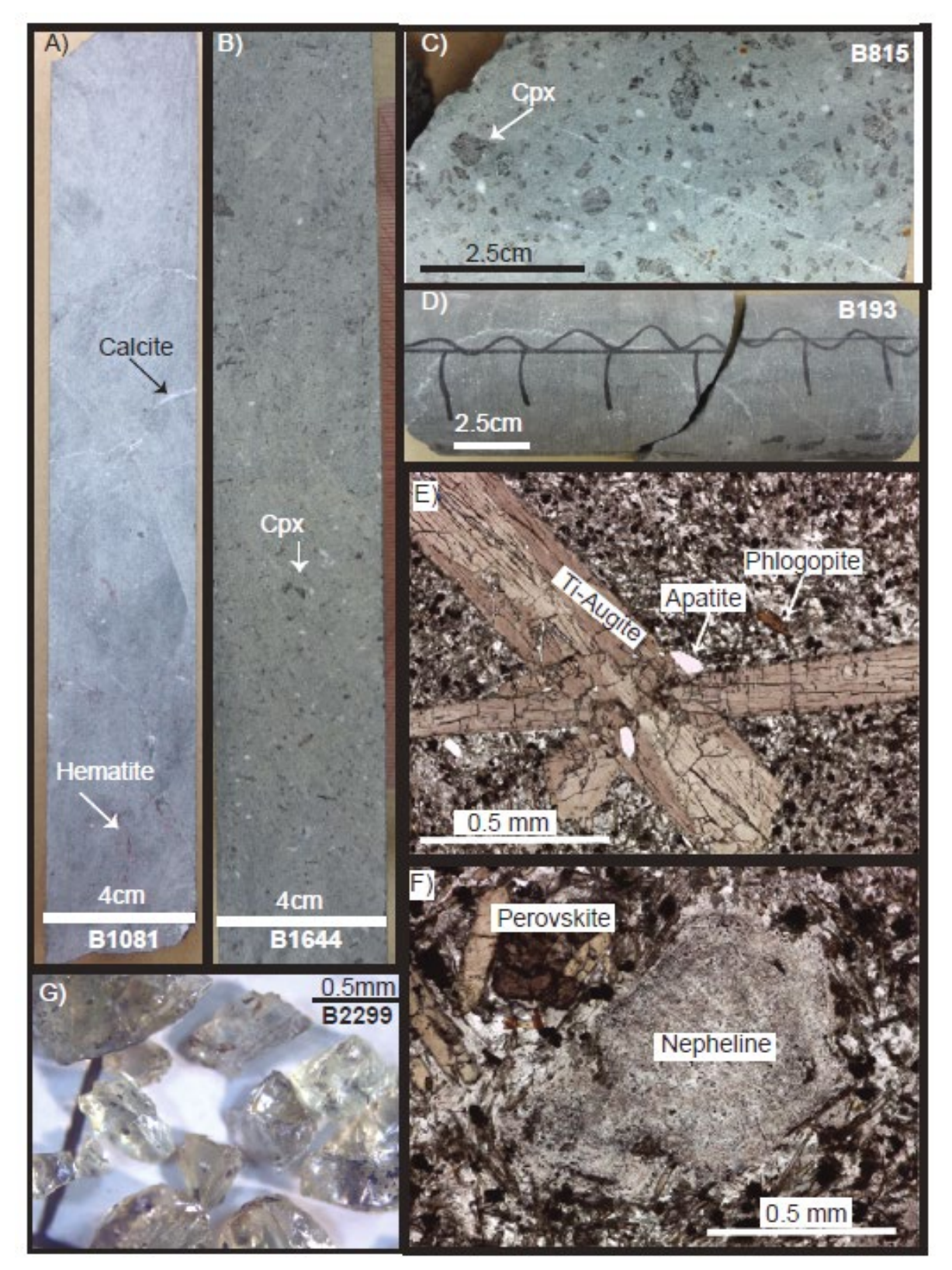
- Haugerud, R. A. & Kunk, M. J. ArAr\*: A Computer Program for Reduction of <sup>40</sup>Ar–<sup>39</sup>Ar Data. Report No. 88-261 (US Geological Survey, 1988).
- Deino, A. L. User's Manual for Mass Spec v. 7.961. Berkeley Geochronology Center Special Publication No. 3 (Berkeley Geochronological Center, Berkeley, 2014).
- Ludwig, K.R. User's Manual for Isoplot 3.75. Berkeley Geochronology Center Special Publication No. 5 (Berkeley Geochronological Center, Berkeley, 2012).
- 74. Min, K., Mundil, R., Renne, P. R. & Ludwig, K. R. A test for systematic errors in 40Ar/39Ar geochronology through comparison with U/Pb analysis of a 1.1-Ga rhyolite. Geochim. Cosmochim. Acta 64, 73–98 (2000).
- Lee, J.-Y. et al. A redetermination of the isotopic abundances of atmospheric Ar. Geochim. Cosmochim. Acta 70, 4507–4512 (2006).
- Moucha, R. & Forte, A. M. Changes in African topography driven by mantle convection. Nat. Geosci. 4, 707–712 (2011).
- Owaga, M. Chemical stratification in a two-dimensional convecting mantle with magmatism and moving plates. J. Geophys. Res. Solid Earth 108, 2561 (2003).
- Duncan, R. A. Age progressive volcanism in the New England seamounts and the opening of the central Atlantic Ocean. J. Geophys. Res. Solid Earth 89, 9980–9990 (1984).
- Willbold, M. & Stracke, A. Trace element composition of mantle end-members: implications for recycling of oceanic and upper and lower continental crust. Geochem. Geophys. Geosyst. 7, Q04004 (2006).
- Mallik, A. & Dasgupta, R. Reactive infiltration of MORB-eclogite-derived carbonated silicate melt into fertile peridotite at 3 GPa and genesis of alkalic magmas. J. Petrol. 54, 2267–2300 (2013).
- Béguelin, P., Bizimis, M., Beier, C. & Turner, S. Rift-plume interaction reveals multiple generations of recycled oceanic crust in Azores lavas. Geochim. Cosmochim. Acta 218, 132–152 (2017).
- Baker, J., Peate, D., Waight, T. & Meyzen, C. Pb isotopic analysis of standards and samples using a <sup>207</sup>Pb–<sup>204</sup>Pb double spike and thallium to correct for mass bias with a double-focusing MC-ICP-MS. *Chem. Geol.* 211, 275–303 (2004).



#### Extended Data Fig. 1 | Geologic map and core log for Bermuda.

**a**, Bathymetric map of the northwestern Atlantic Ocean based on that from ref.  $^{12}$ , highlighting Bermuda and the Bermuda Rise. The predicted westeast hotspot track  $^{78}$  is shown as a red line. **b**, Sketch of the Bermuda core

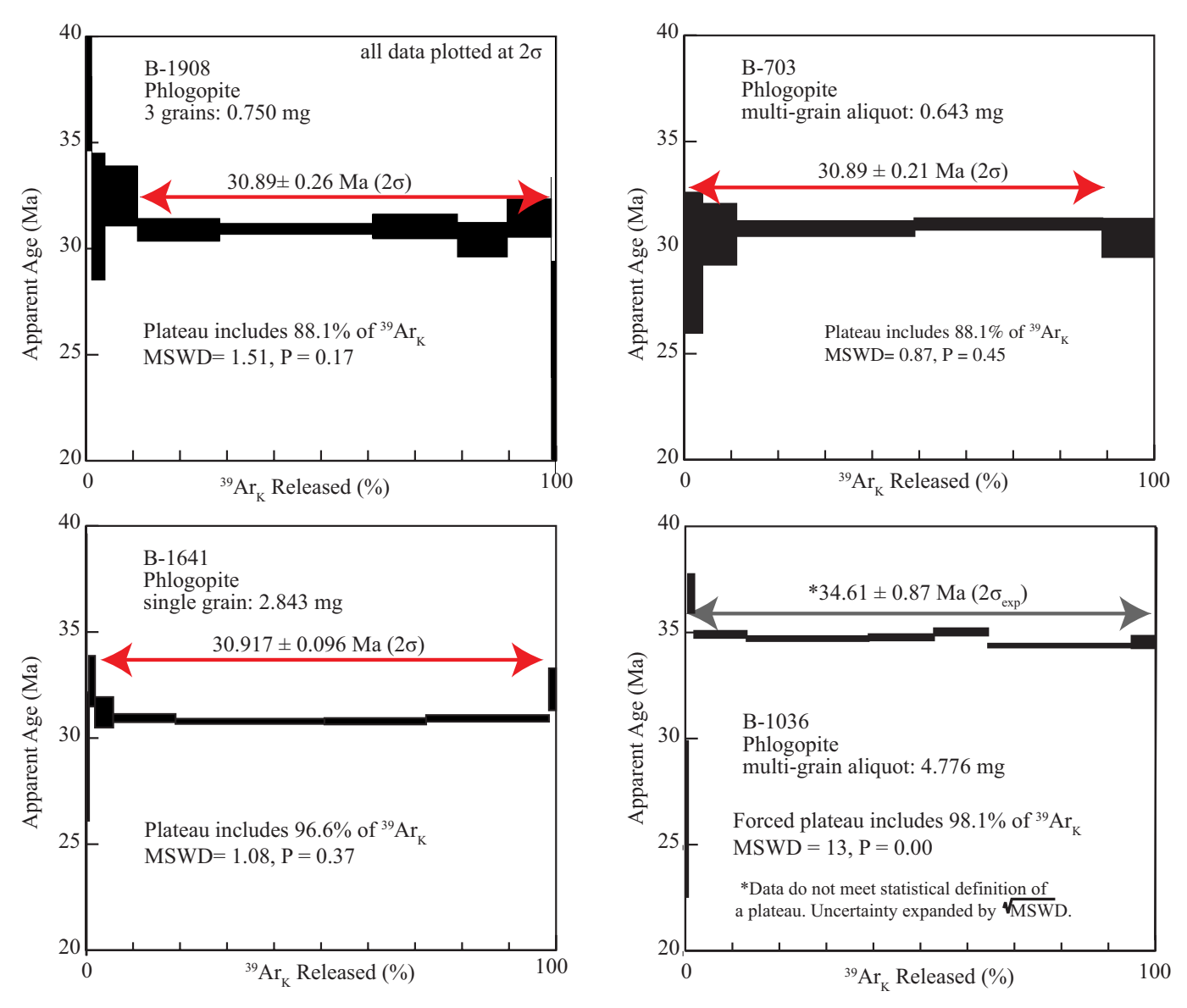
stratigraphy, based on the core log from Dalhousie University. The original core log corresponds to physical markings on the core, all given in inches and feet. Locations at which olivine (O) and phlogopite (Phl) phenocrysts have been observed are marked.



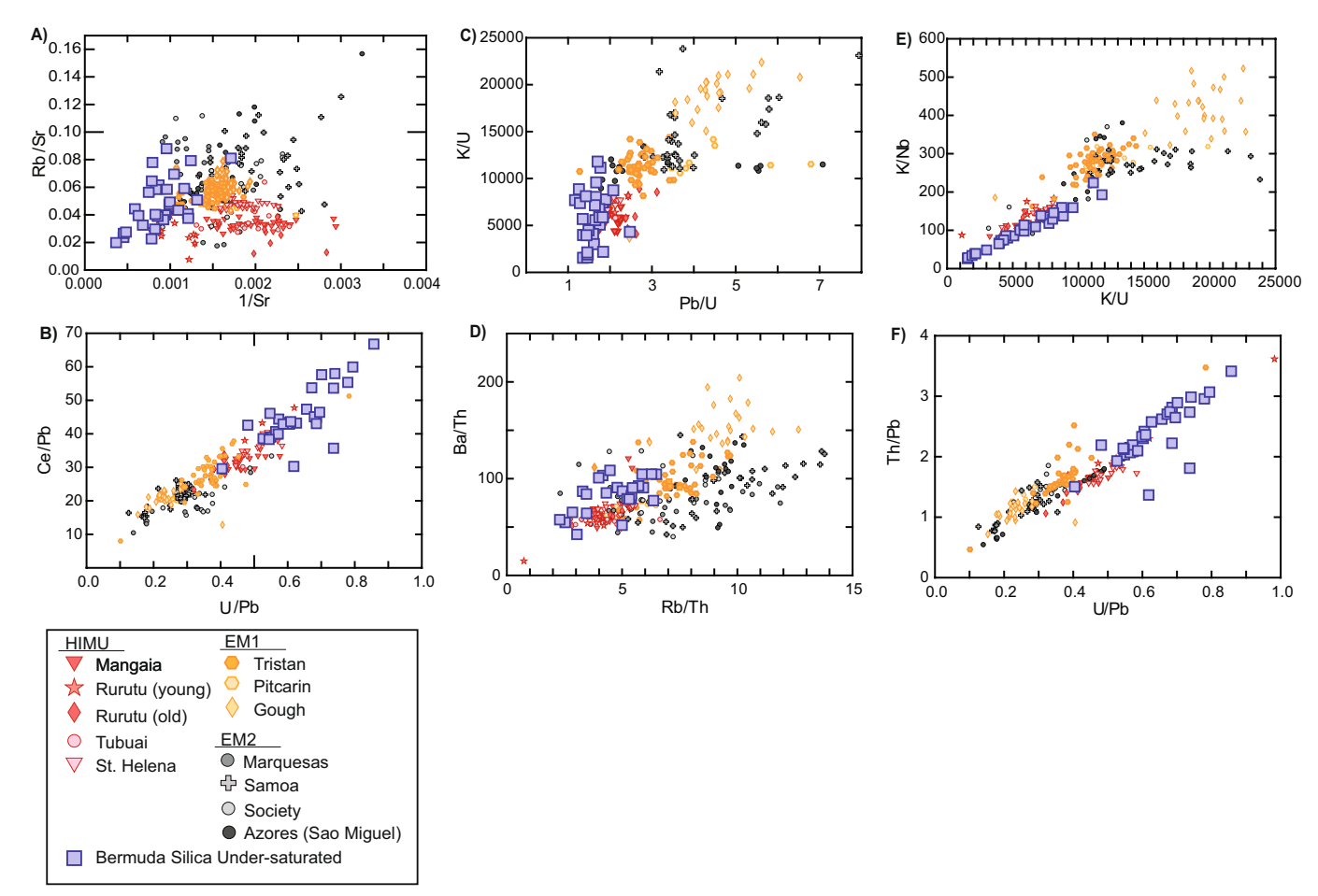
### Extended Data Fig. 2 $\mid$ Examples of samples and mineralogy.

a, Photograph of silica-saturated sample B1081, showing aphanitic texture with haematite and calcite veins. b, Photograph of silica-undersaturated sample B1644 showing porphyritic texture with clinopyroxene (Cpx). c, Photograph of silica-undersaturated sample B815 showing porphyritic texture and large phenocrysts of clinopyroxene (Cpx; up to 1 cm in length).

**d**, Photograph of silica-undersaturated sample B193 showing aphanitic texture. **e**, Micrograph of sample B1908 in cross-polarized light, showing Ti-augite, apatite and phlogopite phenocrysts. **f**, Micrograph of sample B1908 in cross-polarized light, showing perovskite and nepheline phenocrysts. **g**, Olivine separates from B2299.

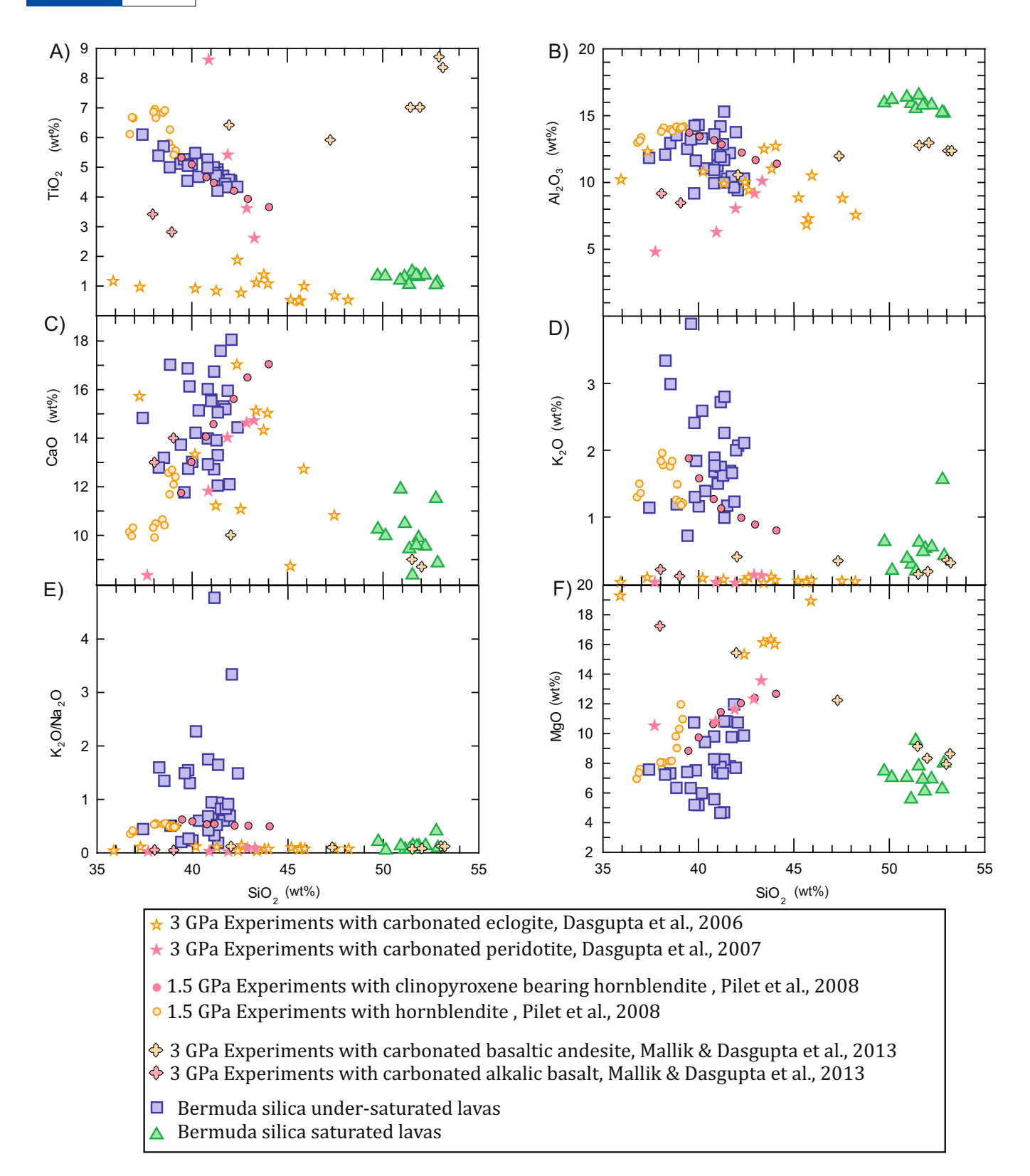


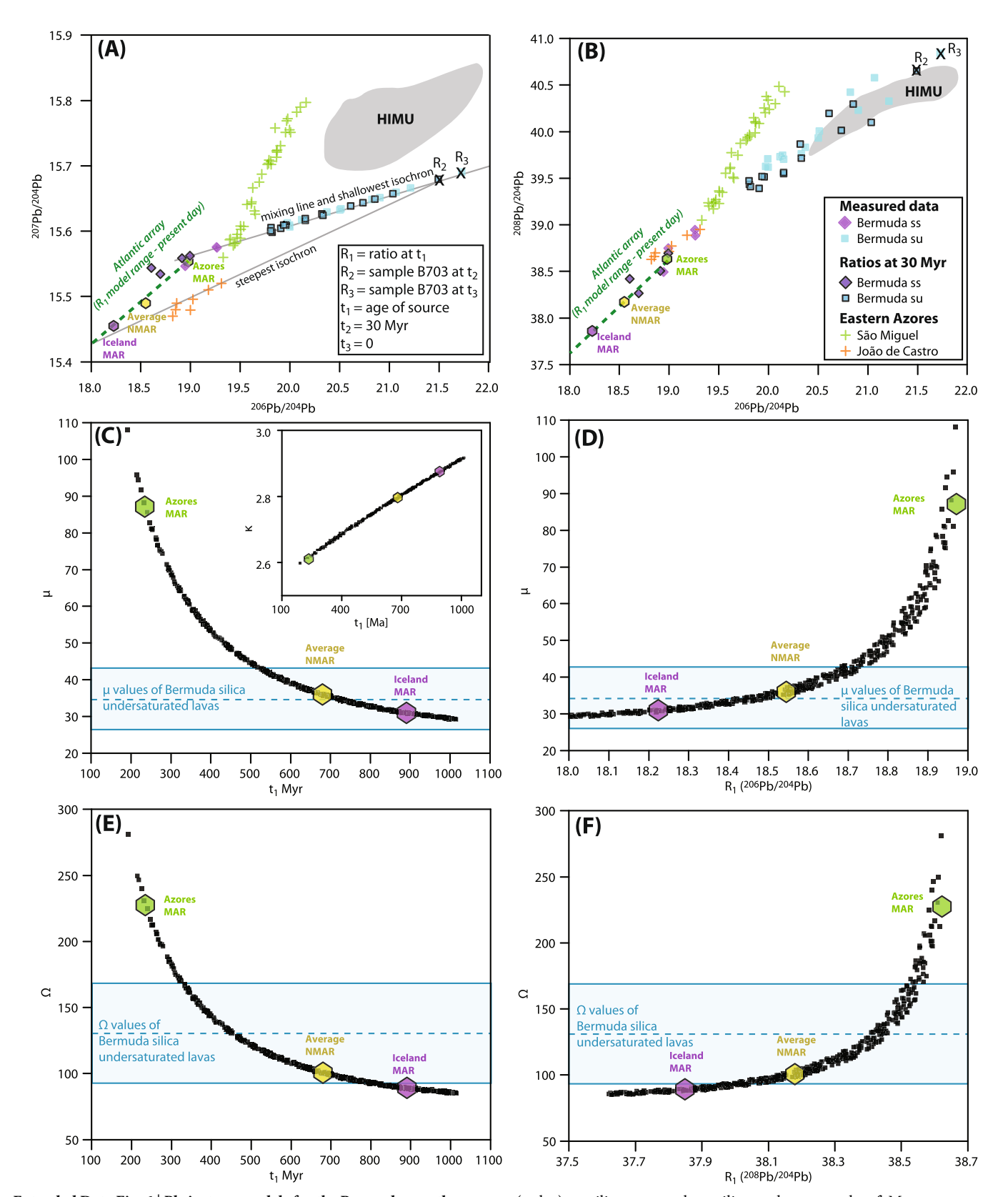
Extended Data Fig. 3 | <sup>40</sup>Ar/<sup>39</sup>Ar age spectra for samples B1908, B703, B1641 and B1036. <sup>40</sup>Ar/<sup>39</sup>Ar step-heating data for silica-undersaturated lavas from Bermuda. The phlogopite phenocrysts age spectrum records a magmatic age of approximately 30.9 Myr.



Extended Data Fig. 4 | Examples of trace-element ratios comparing Bermuda to HIMU, EM1, and EM2 mantle domains from ref. <sup>79</sup>. a, Rb/Sr plotted against 1/Sr, showing Bermuda lavas spanning the range of HIMU, EM1, and EM2 domains. b, Ce/Pb plotted against U/Pb, showing Bermuda lavas as being more enriched than HIMU-derived lavas. c, K/U plotted against Pb/U, showing that Bermuda lavas are K-depleted. d, Ba/Th plotted against Rb/Th, showing that Bermuda lavas

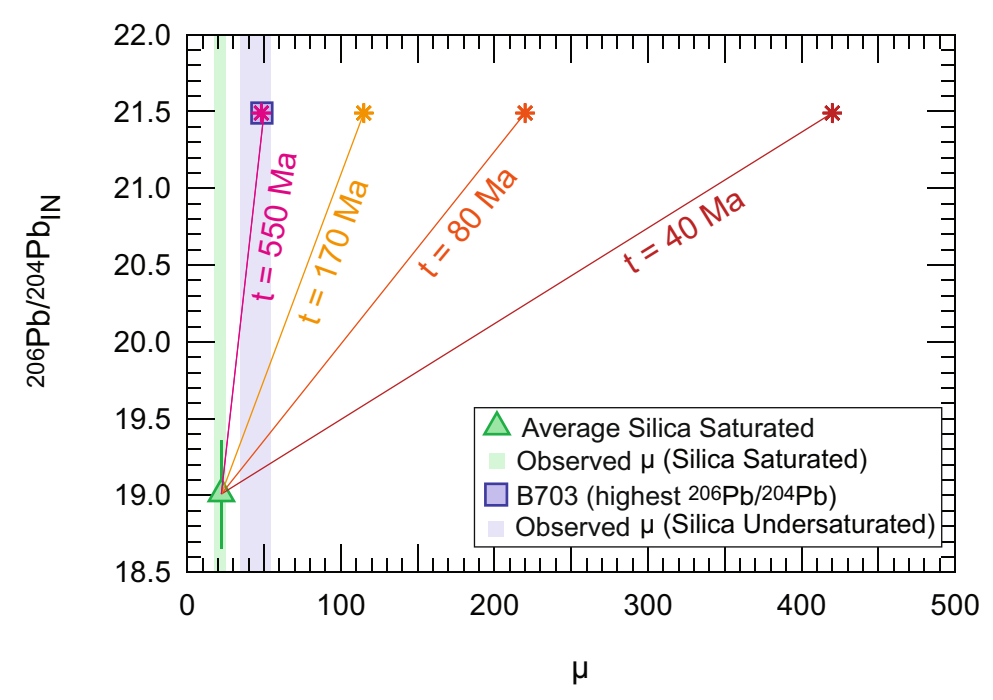
have fluid mobile element ratios similar to those of the HIMU domain. **e**, K/Nb plotted against K/U, showing that Bermuda lavas are K-depleted, with K depletions lower than previously reported for HIMU. **f**, Th/Pb plotted against U/Pb, showing that Bermuda is not characterized by sulfide fractionation, because Th and U are equally enriched and are more enriched than HIMU. EM1, enriched mantle I; EM2, enriched mantle II.





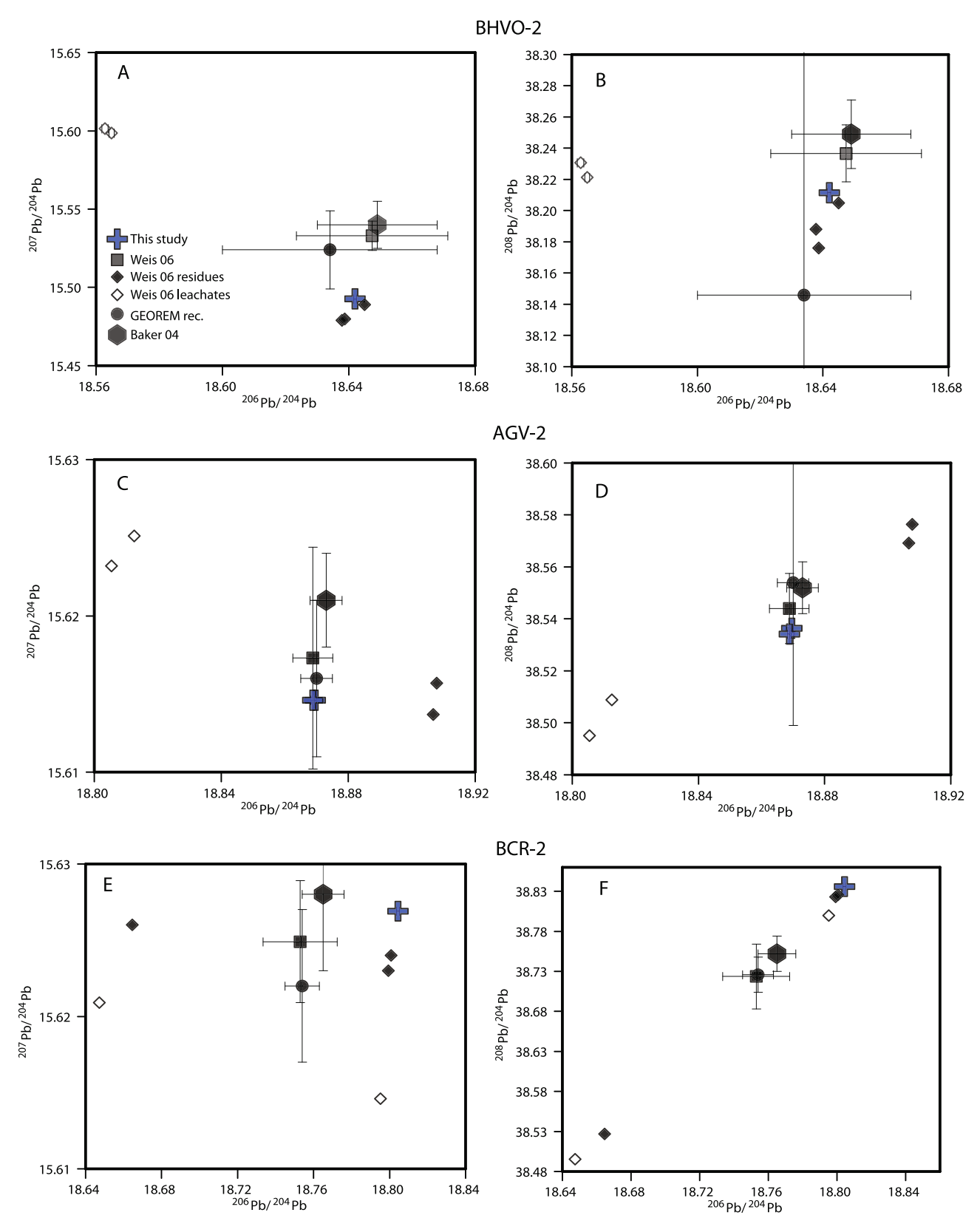
Extended Data Fig. 6 | Pb-isotope models for the Bermuda mantle source. a, b,  $^{206}\text{Pb}/^{204}\text{Pb}-^{207}\text{Pb}/^{204}\text{Pb}$  and  $^{206}\text{Pb}/^{204}\text{Pb}-^{208}\text{Pb}/^{204}\text{Pb}$  plots of Bermuda samples with measured values and age-corrected values (see legend). HIMU<sup>65</sup> and Eastern Azores lavas<sup>81</sup> are plotted for illustration. Azores MAR, Average NMAR and Iceland MAR end members (GEOROC database) are presented along with their linear regression, the Atlantic array.  $R_3$  corresponds to the measured value of sample B703, at  $t_3=0$ 

(today). ss, silica-saturated; su, silica-undersaturated. **c-f**, Monte Carlo results derived from equation (1) for  $R_1$  values falling on the Atlantic array. Azores MAR, Average NMAR and Iceland MAR end members are presented at their respective model values.  $\mu = ^{238}\text{U}/^{204}\text{Pb}$ ,  $\Omega = ^{232}\text{Th}/^{204}\text{Pb}$ ,  $\kappa = ^{232}\text{Th}/^{238}\text{U}$ .  $\mu$  and  $\Omega$  values of Bermuda silica-undersaturated lavas are presented: dashed blue line, average; solid blue lines,  $\pm$  1 s.d.



Extended Data Fig. 7 | Modelling the  $\mu$  of the Bermuda mantle source. Modelled  $\mu$  compositions that are necessary to produce Bermuda's most radiogenic  $^{206}\text{Pb}/^{204}\text{Pb}$  sample (B703) starting from the average composition of the silica-undersaturated, least radiogenic samples. B703 (target) and the average silica-undersaturated samples have been age-corrected to time of eruption (30 Myr ago). Each line corresponds to possible source ages and the necessary  $\mu$  for that source to produce an erupted lava that corresponds to B703. t=40 Myr (70 Myr ago) corresponds to the calculated source age for Bermuda assuming that

Bermuda represents an isochron, with a minimum  $\mu < 420$  necessary. t=80 Myr (110 Myr ago) corresponds both to the error of the Bermuda isochron and the age of the oceanic lithosphere around Bermuda. T=170 Myr (200 Myr ago) corresponds to the rifting of Pangea and the opening of the Atlantic in the region of Bermuda. t=550 Myr (580 Myr ago) corresponds to the ideal source age that can evolve the least radiogenic sample to the most radiogenic sample with a  $\mu$  of 50 (the actual  $\mu$  for B703). Ma, million years ago.



Extended Data Fig. 8 | See next page for caption.



#### Extended Data Fig. 8 | Standard reproducibility for Pb isotopes.

Recommended USGS standard values (BHVO-2, AGV-2 and BCR-2) compared with standards run during this study for <sup>206</sup>Pb/<sup>204</sup>Pb, <sup>207</sup>Pb/<sup>204</sup>Pb, and <sup>208</sup>Pb/<sup>204</sup>Pb. Recommended standard values are from refs <sup>63,82</sup> and the most recent GEOREM preferred values. We did not leach any of our standards. It is important to note that ref. <sup>63</sup> reports that all the USGS standards are variably contaminated during processing, and therefore we plot the residues and leachate data for these USGS standards. **a, b,** Pb isotopes for BHVO-2 showing that our <sup>206</sup>Pb/<sup>204</sup>Pb ratios are within error of the other values, but our <sup>207</sup>Pb/<sup>204</sup>Pb ratios are lower than those in refs <sup>63,82</sup>, yet within error of the GEOREM recommended values

and the residues of leaching from ref. <sup>63</sup>. In ref. <sup>63</sup> it was noted that the BHVO-2 and BHVO-1 are contaminated and that, upon leaching, their residues converge. **c**, **d**, Pb isotopes for AGV-2 showing that our data are within error of those in ref. <sup>63</sup> and the GEOREM recommended values. On the basis of AGV-2, our Pb isotope data are both accurate and highly precise (the duplicates overlap on the symbol size). **e**, **f**, Pb isotopes for BCR-2 showing that our <sup>207</sup>Pb/<sup>204</sup>Pb values are identical to those of refs <sup>63,82</sup>. As in the BHVO-2, our data are closer to the residues of leaching reported in ref. <sup>63</sup>. Ours and literature data plot on a mixing line with the residues of leaching for BCR-2 being highly variable, pointing to heterogeneity in these standards.